

Collision Avoidance Motion Planning for Connected and Automated Vehicle Platoon Merging and Splitting With a Hybrid Automaton Architecture

Shunchao Wang^{ID}, Zhibin Li^{ID}, Bingtong Wang^{ID}, and Meng Li^{ID}

Abstract—Connected and automated vehicle (CAV) platooning exhibits significant potential in enhancing traffic efficiency and sustainability. In unsteady traffic conditions, CAV platoons frequently require splitting and merging maneuvers to avoid obstacles. This study introduces a hybrid automaton architecture for collision avoidance motion planning during CAV platoon merging and splitting. A velocity obstacle algorithm based on potential fields is developed to detect collision risks and calculate collision-free velocity solutions. Two predictive control-based optimization models are developed for collision-avoidance path planning, catering to both single-cruising vehicles and vehicle platoons. A synergistic architecture based on hybrid automaton is developed to coordinate vehicle motions during platoon splitting and merging. Numerical experiments are performed to evaluate the performance of the proposed hybrid automaton architecture under various obstacle scenarios. The results demonstrate that the proposed algorithms effectively identify collision risks within CAV platoons and determine optimal vehicle velocities. The proposed architecture demonstrates excellent performance in adjusting vehicle maneuvers and adapting CAV platoon formations to changing driving environments.

Index Terms—Connected and automated vehicle platoon, collision avoidance, motion planning, hybrid automaton, velocity obstacle, collision risk potential field, model predictive control.

I. INTRODUCTION

COOPERATIVE vehicle platooning, enabled by connected and automated technologies [1], [2], involves virtually-linked vehicles traveling together in a string with short spacing between them. CAV platooning has the potential to achieve significant energy savings and emission reductions [3]. Vehicle maneuvering complexity is greatly reduced, resulting in reduced driver workloads [4], [5]. Maintaining a stable vehicle platoon in actual traffic, especially when encountering obstacles in unstable traffic flow, is challenging [6], [7]. Vehicle platoons frequently require splitting and merging maneuvers to avoid obstacles that disrupt their intended path or motion state [8], [9].

Many studies have investigated the path planning of CAV platoons. Some researchers proposed model predictive control

Manuscript received 29 August 2022; revised 28 June 2023; accepted 7 September 2023. Date of publication 13 October 2023; date of current version 2 February 2024. This work was supported in part by the National Natural Science Foundation of China under Grant 52272331 and Grant 52232012 and in part by the Postgraduate Research and Practice Innovation Program of Jiangsu Province under Grant KYCX21_0131. The Associate Editor for this article was K. C. Leung. (*Corresponding author:* Zhibin Li.)

The authors are with the School of Transportation, Southeast University, Nanjing 210096, China (e-mail: wangshunchao@seu.edu.cn; lizhibin@seu.edu.cn; wangbt@seu.edu.cn; limeng@seu.edu.cn).

Digital Object Identifier 10.1109/TITS.2023.3315063

(MPC)-based algorithms [10], [11], [12], [13], [14], [15], which incorporate safety constraints into a multiobjective optimization framework [16], [17]. These algorithms can effectively guide CAV platoons to avoid obstacles while making minimal adjustments to their desired motion states [18]. However, these algorithms require the implementation of complex optimization solvers, which considerably limit solution efficiency [19], [20]. Optimizing the calculation speed and process to enhance solution efficiency is a significant challenge, particularly when addressing the iterative reinitialization resulting from multi-vehicle state adjustment in vehicle formation [21].

Another research perspective involves determining the collision-avoidance reachability sets of CAV platoons, which include velocities and paths [22], [23], [24], [25], [26]. These methods aim to explore the initial conditions for ensuring platoon safety throughout all subsequent motion times [27], [28]. These algorithms have a simpler solving process compared to the MPC-based optimization methods [29], [30]. However, the estimation of the reachability set tends to be conservative, leading to larger path deviations and traffic delays [21], [31]. Furthermore, in complex road environments, it may be challenging to identify initial conditions that ensure long-term safety [32], [33].

A CAV-platoon controller with guaranteed safety is proposed based on barrier boundary functions. This controller aims to prevent collisions by quantifying the collision risk of the obstacle's radiation areas [34], [35], [36]. The artificial potential field (APF) [37], [38], [39] is a typical representative of barrier boundary functions. APF-based controllers can effectively depict the distribution of collision risks and guide CAV platoons to follow the path with the lowest collision risk [40]. However, existing APF-based controllers fail to accurately characterize the collision risk of moving obstacles because they ignore the differences in risk across different directions [35], [40]. Additionally, when applied over long-term horizons, such controllers are susceptible to generating false alarms because they do not take into account the obstacle's intended trajectories and the maneuver possibilities of vehicles [41], [42].

Moreover, existing methods treat control strategies as relatively independent maneuvers, including platoon keeping, obstacle avoiding, and platoon reconstituting [2], [10]. These controllers cannot fully achieve the cooperative operations of CAV platoons in collision avoidance [8], [20]. For example, when platoons need to be split, these controllers cannot

simultaneously optimize single-vehicle cruising and multi-vehicle platooning. These independent maneuvers lack a synergistic mechanism to ensure the safety and flexibility of CAV platoons.

Furthermore, cooperative platoon control should include collision avoidance for individual vehicles as well as flexible transition during splitting and merging [26], [40]. Existing studies primarily concentrate on trajectory optimization at the platoon level. However, they overlook the cooperative interaction between vehicles and platoons at the system level. Unsmooth transitions during platoon splitting and merging may lead to collisions [36], [43]. Therefore, there is a need to develop a system architecture that enables CAVs to handle the flexible transition of platoon splitting and merging.

The primary objective of this study is to propose a distributed hybrid automaton architecture for the collision avoidance motion planning of CAV platoons. A collision avoidance algorithm that integrates collision risk potential field and velocity obstacle theory is constructed to identify potential collision spaces and collision avoidance solution sets. Two MPC-based motion planning controllers are designed for the path planning and motion tracking of single cruising vehicles and multiple-vehicle platoons. A hybrid automaton-based synergistic architecture with a discrete maneuver transition rule is developed to enable flexible transition and maneuver control of vehicle platoons. This architecture supports various driving modes, including multi-vehicles driving in platoon before splitting, adaptive cruising after splitting, and coordinated driving after reorganization.

This study presents the following contributions:

1) This study proposes a distributed hybrid automaton architecture for the collision avoidance motion planning of CAV platoons, which enables systematic control and flexible transition of vehicle platoon maintenance-splitting-reorganization throughout the entire collision avoidance process.

2) The proposed collision avoidance algorithm effectively integrates the collision risk potential field with velocity obstacle theory, which realizes accurate quantification of the collision risk vector distribution and precise determination of long-term collision avoidance velocities.

3) The proposed motion planning algorithms cooperatively consider the motion requirements of adaptive cruising vehicles and platooning vehicles, which facilitates accurate tracking of collision-avoidance motion states and trajectories of vehicles in different driving states.

The remainder of this paper is organized as follows. Section II introduces the overall framework of the distributed hybrid automaton architecture. The collision detection and avoidance algorithm are presented in Section III. Section IV shows a motion planning and tracking design. A hybrid automaton is developed in Section V. Section VI represents numerical experiments and results. The concluding remarks can be found in the final section.

II. OVERALL ARCHITECTURE

A. Overall Framework

The hybrid automaton architecture incorporates a switching logic between two maneuvers: single-vehicle cruising

and multiple-vehicle platooning. The hybrid automaton architecture, as depicted in Fig. 1, comprises three functional components: 1) system collaboration and operation, 2) collision detection and avoidance, and 3) path planning and tracking. The functions of each functional component are outlined as follows:

1) System collaboration and operation acts as the coordination center for all functional modules. It establishes the state sets and operation modes of the control architecture. In particular, the system state set defines the motion states of vehicles and obstacles. The system operation mode establishes the maneuver transition rules for single-vehicle cruising and multiple-vehicle platooning. It also determines the event-trigger rules for platoon splitting and merging.

2) Collision detection and avoidance serves as the risk-perception module within the control architecture. It is responsible for detecting collision risks and generating collision-avoidance solutions by analyzing the combined information from vehicle motion states and traffic conditions. Specifically, the collision risk potential field (CRPF) is utilized to quantify collision risks associated with obstacles. The velocity obstacle model is developed to identify collision velocities that result in high collision risk. The dynamic window approach is designed to determine collision-free velocities.

3) Path planning and tracking functions as the path optimization module within the control architecture. Its objective is to update vehicle motion states and generate collision avoidance paths. It is designed to facilitate the transition between two distinct maneuvers: single-vehicle cruising and multiple-vehicle platooning. Specifically, the vehicle dynamic model is utilized to represent vehicle motion states. Two model predictive control (MPC)-based models are developed to track collision-avoidance trajectories for single-cruising vehicles and multiple-vehicle platoons.

B. System Assumption

Due to the integration of intelligent connected technologies such as DSRC, C-V2X, 5G/6G-V2X, the connected and automated control system enables real-time or near real-time transmission and control of information [25], [26], [27], [28], [29], [34], [35], [36], [40], [41], [42]. Therefore, the proposed hybrid automaton architecture is designed and implemented based on the following assumptions:

1) Road system: CAVs operate on a road system equipped with advanced networking technologies and infrastructure. The road system is equipped with comprehensive facilities and equipment for information perception, transmission, computation, storage, control, and other related functions.

2) Information communication: CAVs have the ability to perceive, transmit, and receive real-time driving environment and vehicle control information. The information communication is either free from delay or the delay is negligible.

3) Vehicle control: CAVs are capable of making precise adjustments to their driving behavior and motion maneuvers. They can engage in adaptive cruise driving or form platoons with other CAVs. The CAV platoon utilizes distributed control,

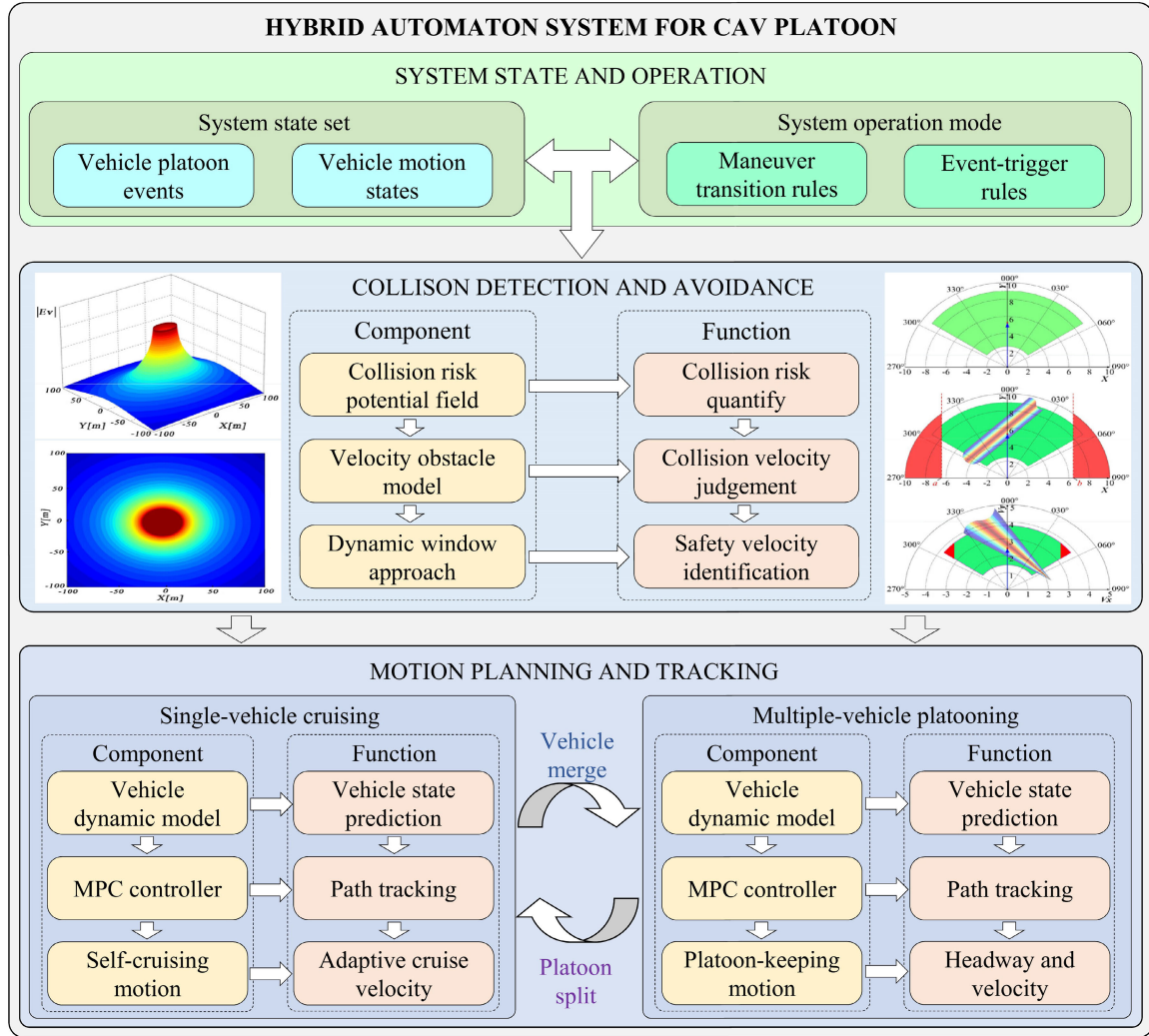


Fig. 1. Controller framework of the CAV hybrid automaton system.

allowing each CAV to autonomously control its behavior according to dynamic conditions.

III. COLLISION DETECTION AND AVOIDANCE

A. Collision Risk Detection by Velocity Obstacle

The Velocity Obstacle (VO) aims to identify velocities that result in collisions between the subject vehicle and the obstacle vehicle [44], [45]. By considering velocity variations at continuous times, VO help eliminate nuisance alerts associated with long-term horizons [46]. Additionally, VO can reduce the computational effort of motion controllers by identifying collision velocities over the long term [42].

VO defines a collision as the subject vehicle and the obstacle vehicle simultaneously appearing in the same position at a future time t_f , i.e.,

$$\exists t_f \in t, P_S(t_f) = P_S(t_0) + v_S(t_f - t_0) = P_O(t_f) \quad (1)$$

where, $P_S(t_f)$ and $P_O(t_f)$ denote the positions of the subject vehicle and the obstacle vehicle at time t_f , respectively; $P_S(t_0)$ is the position of the subject vehicle at time t_0 ; v_S is the velocity of the subject vehicle.

The possible collision position is not one point ($P_O(t_f)$) because the vehicle is a shaped entity. It should be an area covered by vehicles' geometric bodies. The area contains all points with the cumulative shape of the subject vehicle and the obstacle vehicle. Thus, Equation (1) should be represented as [47].

$$P_S(t_0) + v_S(t_f - t_0) \in P_O(t_f) \oplus \text{Conf}P(S, O) \quad (2)$$

where, \oplus denotes a Minkowski addition; $\text{Conf}P(S, O)$ denotes the positions covered by the vehicle, for example, if the subject vehicle and the obstacle vehicle are seen as two circles with radii r_S and r_O , the $\text{Conf}P(S, O)$ is the point set covered by an expanding circle with a radius $r_S + r_O$,

$$\text{Conf}P(S, O) = \{P | \|P - O\| \leq r_S + r_O\} \quad (3)$$

where, P denotes a possible collision point, O is the centroid of the obstacle vehicle.

Solving Equation (2) regarding v_S , it turns out to be

$$v_S = \frac{P_O(t_f) - P_S(t_0)}{t_f - t_0} \oplus \frac{\text{Conf}P(S, O)}{t_f - t_0} = s\text{VO}(t_f) \quad (4)$$

Equation (4) collects a velocity set of the subject vehicle leading to a collision at a time slice t_f . A set of collision

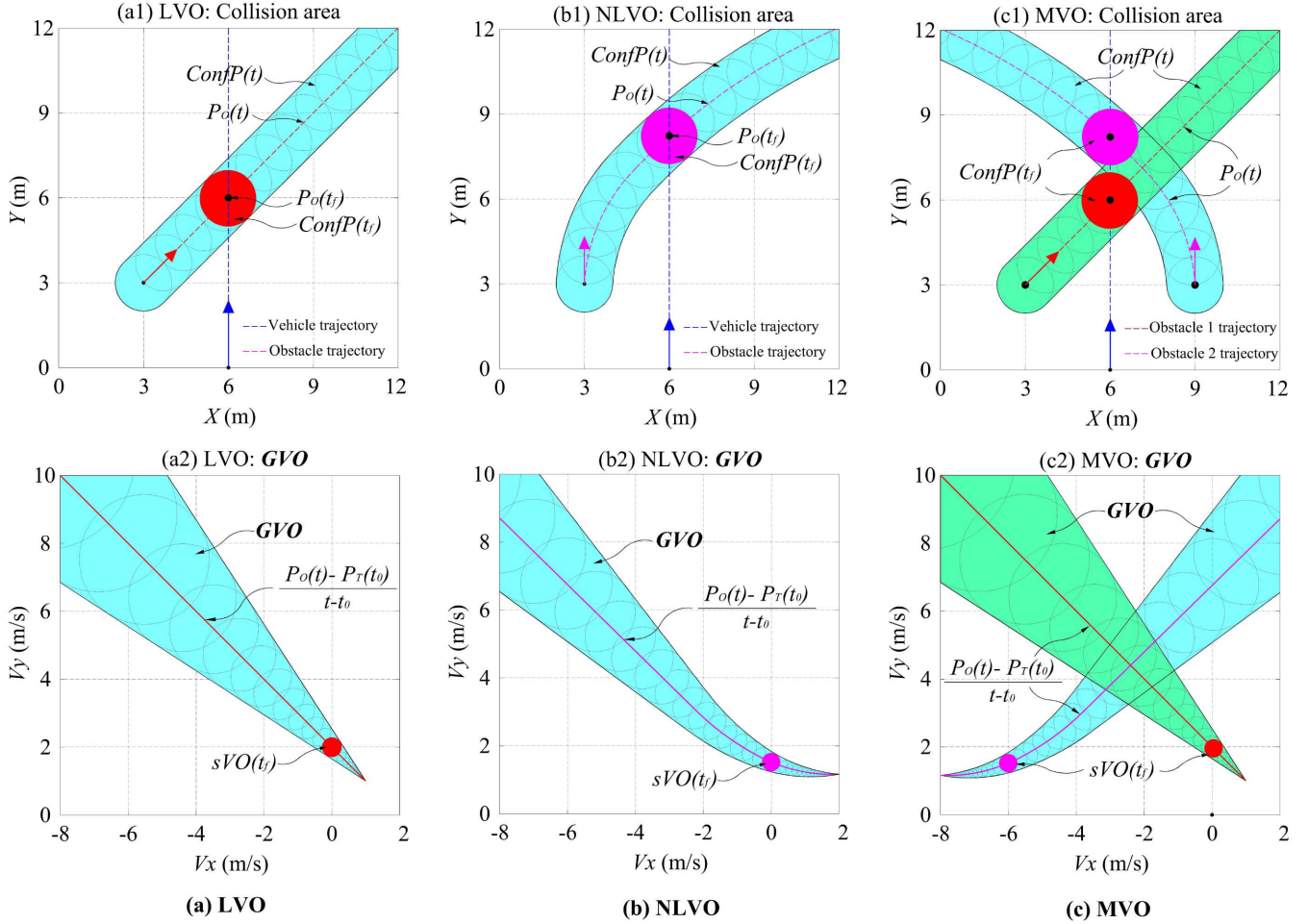


Fig. 2. Illustration of collision area and collision velocity set of LVO, NLVO and MVO.

velocities at any time t is a union of $sVO(t)$, where $t \in (t_0, \infty)$,

$$\begin{aligned} GVO &= \bigcup_t^{\infty} sVO(t) \\ &= \bigcup_t^{\infty} \left(\frac{P_O(t) - P_S(t_0)}{t - t_0} \oplus \frac{ConfP(S, O)}{t - t_0} \right) \quad (5) \end{aligned}$$

A velocity in this set (**GVO**) means that the subject vehicle is guaranteed to collide with the obstacle vehicle at a future time ($t_0 \rightarrow \infty$). Fig. 2 gives some demonstrations of $ConfP(S, O)$ and **GVO** set of velocity obstacles. Linear velocity obstacle (LVO) is caused by an obstacle with a constant velocity, while nonlinear velocity obstacle (NLVO) is caused by an obstacle with changing velocities. The multiple velocity obstacle (MVO) is caused by multiple obstacles. The subject vehicle will collide with the obstacle vehicle if its position and velocity fall into the collision areas and collision velocity sets.

B. Collision Risk Quantification by CRPF

Obstacle vehicle's geometric body cannot accurately measure the collision risk of the collision area $ConfP(S, O)$. The collision risk is different for moving obstacle vehicles in different directions and distances [37,40]. The red circle $ConfP(t_f)$ and $sVO(t_f)$ in Fig. 2 cannot precisely represent

the collision risk of a moving vehicle [39,41]. A CRPF is introduced to refine the collision area. An obstacle vehicle's CRPF can be defined by its physical attributes, motion states, road conditions, and the vector distances between vehicles [42].

- **Vehicle Virtual mass.** Obstacles with greater mass and speed pose a higher collision risk. The concept of virtual mass is introduced to capture the impact of the obstacle vehicle's mass and speed [48],

$$M = m \cdot \left(1.566 \times 10^{-14} \cdot v^{6.687} + 0.3354 \right) \quad (6)$$

where, m and v are the real mass and speed of the obstacle vehicle, respectively.

- **Vehicle type.** Trucks commonly exhibit higher collision risks compared to passenger cars. A vehicle attribute indicator is defined to capture the collision risk disparities arising from vehicle type,

$$T = \left(\frac{s}{s^*} \right)^{\varpi_1} \cdot \left(\frac{\kappa}{\kappa^*} \right)^{\varpi_2} \quad (7)$$

where, s and κ is vehicle size and the object type it carries. s^* and κ^* is the standard values, i.e., small car and people. ϖ_1 and ϖ_2 are undetermined constants.

- **Pseudo distance.** Vehicles within the same lane pose a greater collision risk compared to vehicles in adjacent lanes. A shorter distance indicates a more hazardous situation

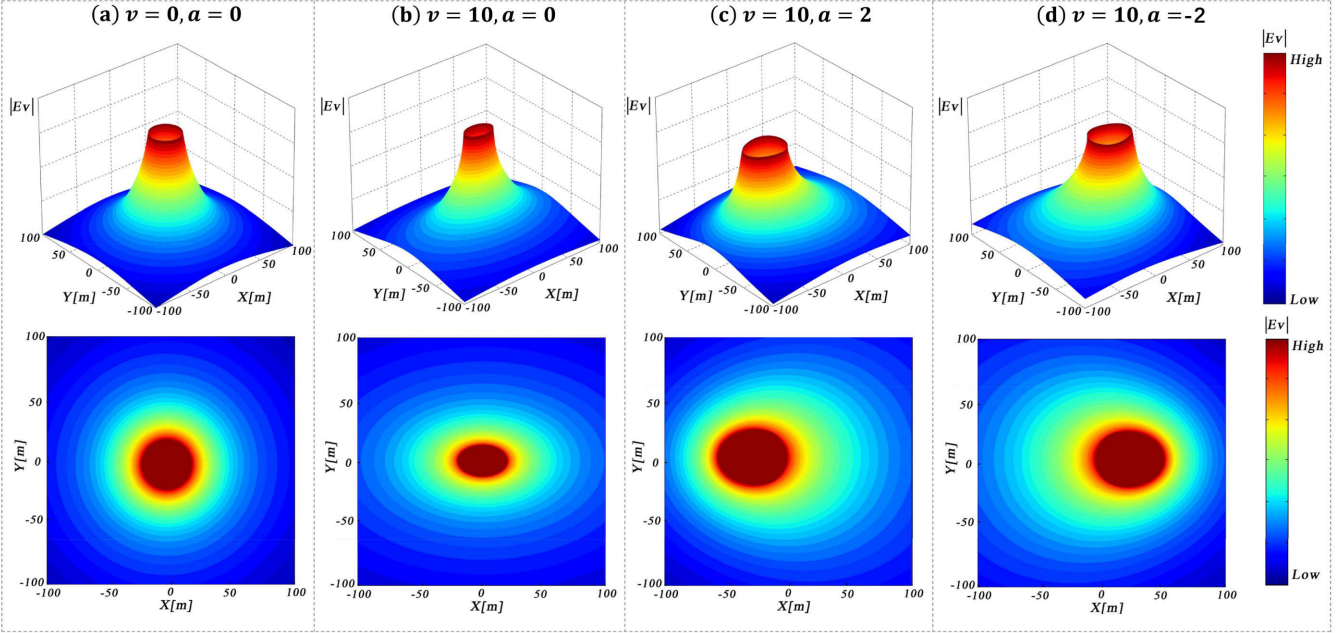


Fig. 3. Illustration of the CRPF given by Equation 11 (set $G = 0.5$, $R = 1$, $K = 5$, $T = 1$, $\zeta = 1.2$).

compared to a longer distance. A pseudo distance is introduced to capture the impact of motion direction and distance on collision risk,

$$r_d = \sqrt{[(x_s - x_o) \varepsilon \cdot \exp(-\rho v)]^2 + [(y_s - y_o) \varepsilon]^2} \quad (8)$$

where, (x_s, y_s) and (x_o, y_o) are the positions of the subject vehicle and the obstacle vehicle, ε and ρ are the undetermined coefficients.

• **Acceleration.** The collision risk is greater in the direction of acceleration compared to other directions. An acceleration indicator is introduced to capture the impact of acceleration,

$$\phi = \frac{K}{K - |\mathbf{a}| \cos \vartheta_a} \quad (9)$$

where, \mathbf{a} is the acceleration vector of the obstacle vehicle, ϑ_a is the clockwise angle between the direction of \mathbf{a} and \mathbf{r}_d , K is the undetermined coefficient ($K > 0$).

• **Road conditions.** Positions with poor road conditions are more prone to vehicle accidents. A road indicator is defined to express the influence of road conditions as Equation (10).

$$R = \left(\frac{\xi}{\xi^*} \right)^{\gamma_1} \cdot \left(\frac{\mu}{\mu^*} \right)^{\gamma_2} \cdot \exp [(\varrho - \varrho^*)^{\gamma_3} + (\tau - \tau^*)^{\gamma_4}] \quad (10)$$

To sum up, the CRPF is represented based on the expression of Yukawa potential [49], as shown in Equation (11). Fig. 3 illustrates the CRPF of obstacles in various motion states. The centroid of the CRPF represents the center of the obstacle vehicle. The color depth corresponds to the level of collision risk. CRPF equipotential lines are formed by points with the same collision risk. Each equipotential line represents a collision area, denoted as $Conf P(S, O)$, associated with a specific level of collision risk.

$$E_V = \frac{GMT R \phi}{|\mathbf{r}_d|^\zeta} \cdot \frac{\mathbf{r}_d}{|\mathbf{r}_d|} = \left(1.566 \times 10^{-14} \cdot v^{6.687} + 0.3354 \right)$$

$$\cdot \frac{KGTRm}{(K - |\mathbf{a}| \cos \vartheta_a) \cdot |\mathbf{r}_d|^\zeta} \cdot \frac{\mathbf{r}_d}{|\mathbf{r}_d|} \quad (11)$$

where, ξ and ξ^* , μ and μ^* , ϱ and ϱ^* , τ and τ^* are the actual and standard values of the road visibility, friction coefficient, curvature, and slope, G and ζ are the undetermined coefficients ($G, \zeta > 0$).

C. Collision Risk Avoidance by Dynamic Window Approach

A certain level of collision risk can be avoided by adjusting subject vehicle's velocity out of the collision velocity set $GVO(E_V^i)$,

$$v_S \notin GVO(E_V^i) \\ = \bigcup_t^{\infty} \left(\frac{P_O(t) - P_S(t_0)}{t - t_0} \oplus \frac{Conf P(E_V^i)}{t - t_0} \right) \quad (12)$$

where, E_V^i denotes the i th level collision risk; $GVO(E_V^i)$ represents the collision velocity set that leads to the collision risk E_V^i ; $Conf P(E_V^i)$ denotes the area with collision risk E_V^i .

Due to the limitation of the vehicle dynamics and the driving rules, not all velocities defined by Equation (12) are achievable in a limited time. Fig. 4 illustrates the candidate positions and velocities modeled by the dynamic window approach [50], [51]. The dynamic state can be discretized as follows.

$$\chi(t) = \begin{bmatrix} v_x(t) \\ v_y(t) \\ \theta(t) \\ x(t) \\ y(t) \end{bmatrix} = \begin{bmatrix} v_x(t_0) + \Delta t \cdot \dot{v}(t_0) \sin \theta_{t_0} \\ v_y(t_0) + \Delta t \cdot \dot{v}(t_0) \cos \theta_{t_0} \\ \theta(t_0) + \Delta t \cdot \dot{\theta}(t_0) \\ x(t_0) + \Delta t \cdot v_x(t_0) \\ y(t_0) + \Delta t \cdot v_y(t_0) \end{bmatrix} \quad (13)$$

where, χ denotes vehicle state vector; $x(t_0)$ and $x(t)$, $y(t_0)$ and $y(t)$, $v_x(t_0)$ and $v_x(t)$, $v_y(t_0)$ and $v_y(t)$, $\theta(t_0)$ and $\theta(t)$ denote the lateral position, longitudinal position, lateral velocity, longitudinal velocity, and direction angle at time

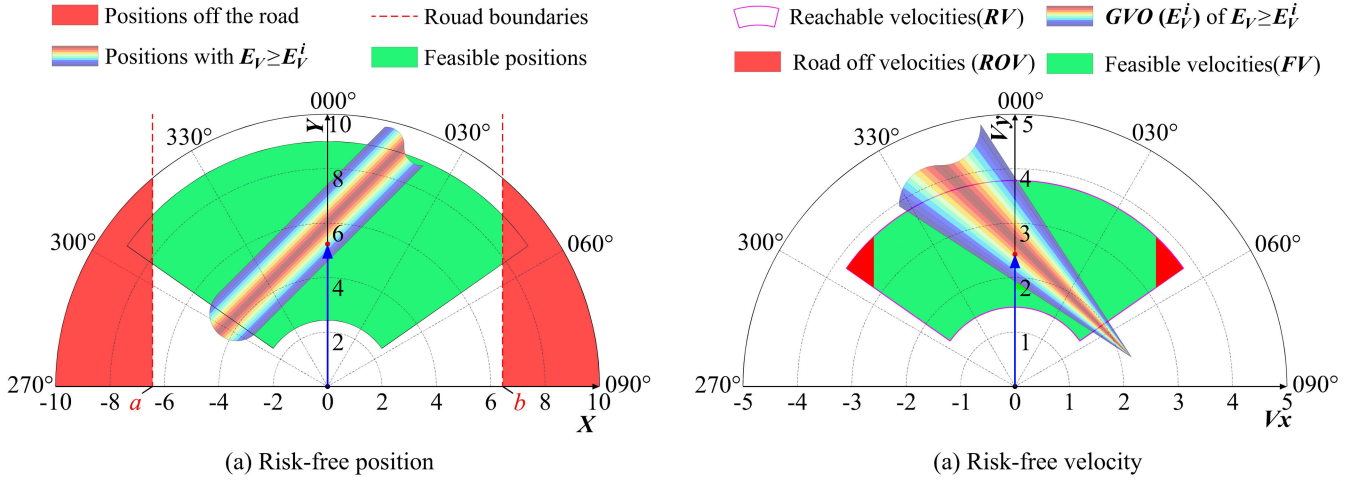


Fig. 4. Illustration of collision-avoidance velocity calculated by dynamic window approach.

t_0 and time t , respectively; \dot{v} and $\dot{\theta}$ are the linear acceleration and angular acceleration.

The subject vehicle should not drive off the drivable area, such as the whole road or a designated lane. The velocities that cause the subject vehicle to leave road boundaries can be defined as Equation (14).

$$\mathbf{ROV} = \left\{ v(t) \mid \begin{array}{l} x(t_0) + v_x(t_0) \frac{v(t) - v(t_0)}{\dot{v}} \leq a \\ x(t_0) + v_x(t_0) \frac{v(t) - v(t_0)}{\dot{v}} \geq b \end{array} \right\} \quad (14)$$

where, \mathbf{ROV} denotes a set of velocities that cause the subject vehicle to leave the drivable area; a and b are the boundaries of the drivable area.

The velocities that the subject vehicle can achieve in a limited time are expressed as Equation (15), shown at the bottom of the next page. The feasible velocities that meet the requirements of collision avoidance, vehicle dynamics, and driving rules can be obtained as Equation (16), shown at the bottom of the next page.

where, \mathbf{RV} denotes the reachable velocity set; \dot{v}_{min} and \dot{v}_{max} , $\dot{\theta}_{min}$ and $\dot{\theta}_{max}$ denote the minimum/maximum linear acceleration and the minimum/maximum angular acceleration, \mathbf{FV} is the feasible velocity set.

The velocity in the feasible velocity set can guide the subject vehicle to avoid the i th level collision risk \mathbf{E}_V^i . Additionally, a feasible velocity set for avoiding lower-/higher-level collision risks can be obtained by expanding/reducing \mathbf{GVO} area in Fig. 4(b).

IV. MOTION PLANNING AND TRACKING

A. Vehicle Dynamics Model-Based Motion Modeling

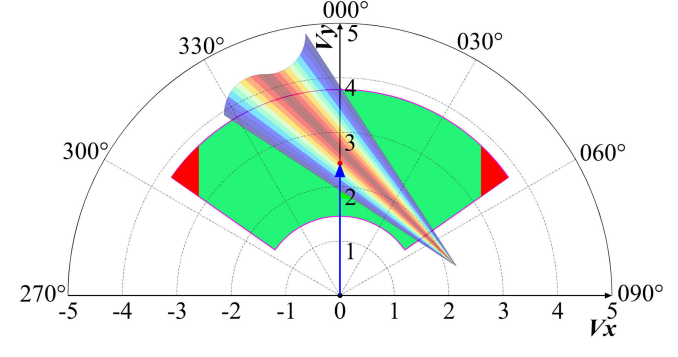
This section exploits the dynamics equations to model vehicle motion states. Fig. 5 depicts a diagram of the model with the longitudinal, lateral, and yaw degrees of freedom,

$$m \cdot (\dot{v}_y - v_x r) = F_{yt} \quad (17)$$

$$m \cdot (\dot{v}_x + v_y r) = F_{xf} + F_{xr} \quad (18)$$

$$I_Z \dot{r} = F_{xf} l_f - F_{xr} l_r \quad (19)$$

Reachable velocities(RV) \mathbf{GVO} (\mathbf{E}_V^i) of $\mathbf{E}_V \geq \mathbf{E}_V^i$
Road off velocities (ROV) Feasible velocities (FV)



(a) Risk-free position

The vehicle's motion with respect to global coordinates is defined as follows

$$\dot{X} = v_y \sin \theta + v_x \cos \theta \quad (20)$$

$$\dot{Y} = v_y \cos \theta + v_x \sin \theta \quad (21)$$

where, X and Y are the vehicle lateral and longitudinal positions; θ denotes vehicle direction angle; v_x and v_y represent vehicle lateral/longitudinal velocities; r represents vehicle yaw rate at CG (center of gravity); I_Z is the vehicle moment of inertia; l_r and l_f represent the distance from the vehicle CG to the rear and front axles; F_{yt} is the total tires longitudinal force; F_{xf} and F_{xr} are the total lateral forces of the front and rear tires, respectively.

The vehicle is assumed to have a front steering system. Utilizing a linear tire model, the lateral forces are developed as

$$F_{xf} = -C_f \alpha_f = C_f \left(\delta - \frac{v_x + l_f r}{v_y} \right) \quad (22)$$

$$F_{xr} = -C_r \alpha_r = C_r \left(-\frac{v_x - l_r r}{v_y} \right) \quad (23)$$

where, α_f and α_r denote the front and rear tires sideslip angles; δ is the front steering angle; C_f and C_r represent the cornering stiffness of the front and rear tires, respectively.

The linear dynamics can then be obtained by linearizing Equation (14)-(20) around the vehicle's operating point. The state vector can be defined as $\mathbf{X} = [Y \ v_y \ X \ v_x \ \theta \ r]^T$, the control input is $\mathbf{Z} = [F_{yt} \ \delta]^T$, and the control output is $\mathbf{Y} = [X \ v_y \ \theta]^T$. Thus,

$$\dot{\mathbf{X}} = \mathbf{A}\mathbf{X} + \mathbf{B}\mathbf{Z} \quad (24)$$

$$\mathbf{Y} = \mathbf{C}\mathbf{X} \quad (25)$$

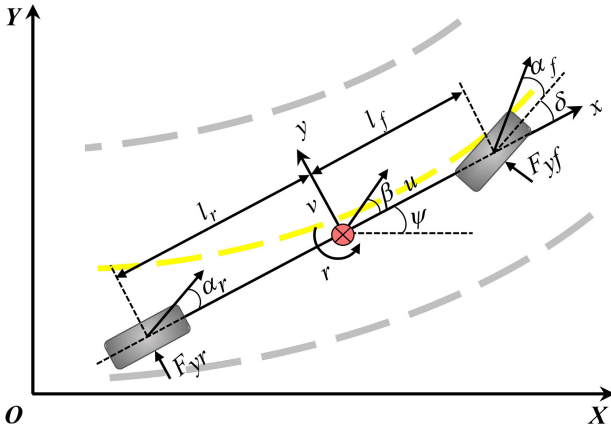


Fig. 5. Vehicle model for motion driving and path tracking.

where,

$$\begin{aligned} \mathbf{A} &= \begin{bmatrix} 0 & 1 & 0 & 0 & 0 & 0 \\ 0 & 0 & 0 & 0 & 0 & 0 \\ 0 & 0 & 0 & 1 & v_y & 0 \\ 0 & 0 & 0 & -\frac{C_f + C_r}{mv_y} & 0 & \frac{l_r C_r - l_f C_f}{mv_y} - v_y \\ 0 & 0 & 0 & 0 & 0 & 1 \\ 0 & 0 & 0 & \frac{l_r C_r - l_f C_f}{l_z v_y} & 0 & -\frac{l_r^2 C_r + l_f^2 C_f}{l_z v_y} \end{bmatrix} \\ \mathbf{B} &= \begin{bmatrix} 0 & \frac{1}{m} & 0 & 0 & 0 & 0 \\ 0 & 0 & 0 & \frac{C_f}{m} & 0 & \frac{l_f C_f}{l_z} \end{bmatrix}^T \\ \mathbf{C} &= \begin{bmatrix} 0 & 0 & 1 & 0 & 0 & 0 \\ 0 & 1 & 0 & 0 & 0 & 0 \\ 0 & 0 & 0 & 0 & 1 & 0 \end{bmatrix} \end{aligned}$$

To predict the control outputs in a finite horizon N_P , the above linear dynamics can be discretized to an incremental prediction model by using the Tustin algorithm [52]

$$\Delta \mathbf{\bar{X}}(k+1) = \mathbf{A}_k \Delta \mathbf{\bar{X}}(k) + \mathbf{B}_k \Delta \mathbf{\bar{Z}}(k) \quad (26)$$

$$\mathbf{\bar{Y}}(k) = \mathbf{C}_k \Delta \mathbf{\bar{X}}(k) + \mathbf{\bar{Y}}(k-1) \quad (27)$$

where, $\Delta \mathbf{\bar{X}}(k) = \mathbf{\bar{X}}(k) - \mathbf{\bar{X}}(k-1)$, $\Delta \mathbf{\bar{Z}}(k) = \mathbf{\bar{Z}}(k) - \mathbf{\bar{Z}}(k-1)$.

The prediction output vector within the prediction horizon N_P and control input increment vector within the control horizon N_C ($N_P > N_C$) can be defined as follows

$$\begin{aligned} \mathbf{\bar{Y}}_{N_p}(k) &= [\mathbf{\bar{Y}}(k+1) \ \mathbf{\bar{Y}}(k+2) \ \dots \ \mathbf{\bar{Y}}(k+N_p)]^T_{1 \times N_p} \quad (28) \end{aligned}$$

$$\begin{aligned} \Delta \mathbf{\bar{Z}}_{N_c}(k) &= [\Delta \mathbf{\bar{Z}}(k) \ \Delta \mathbf{\bar{Z}}(k+1) \ \dots \ \Delta \mathbf{\bar{Z}}(k+N_c-1)]^T_{1 \times N_c} \quad (29) \end{aligned}$$

B. Model Predictive Control-Based Motion Planning

The motion planning task can be posed as a predictive tracking control problem with constraints. The action

sequence of the desired control inputs and output defined by Equation (26)-(29) are generated and updated by repeatedly solving finite-time optimal control problems in a receding horizon fashion in an MPC scheme [53], [54]. The open-loop optimal problem with the cost function and operating constraints are solved over a finite horizon at each time step.

Fig. 6 displays a collision-avoidance scenario for the CAV platoon. The single-cruising vehicle only seeks the lowest risk path to keep itself in the desired motion state. The platooning vehicles need to keep themselves in unified movements with their preceding vehicles. The transition of vehicle maneuvers corresponds to the switching of the motion objectives. Different control models are set for the single-cruising vehicle and the platooning vehicle. The cost functions are defined for the two vehicle types as J_{crus} and J_{pltn} .

$$\begin{aligned} \min J_{crus}(\mathbf{\bar{X}}(k), \Delta \mathbf{\bar{Z}})(k) \\ = \min_{\mathcal{Z}_{Nc}, \varepsilon} \sum_{k=1}^{N_P} \mathbf{E}_{v(k)} \\ + \|\mathbf{Y}_{N_p}(k) - \mathbf{Y}_{des}(k)\|_{\mathbf{Q}}^2 + \|\Delta \mathbf{\bar{Z}}_{N_c}(k)\|_{\mathbf{R}}^2 \\ + \|\varepsilon_k\|_{\mathbf{P}}^2 \end{aligned} \quad (30)$$

$$\begin{aligned} \min J_{pltn}(\mathbf{\bar{X}}(k), \Delta \mathbf{\bar{Z}})(k) \\ = \min_{\mathcal{Z}_{Nc}, \varepsilon} \sum_{k=1}^{N_P} \mathbf{E}_{v(k)} \\ + \sum_{k=1}^{N_P} \|X(k) - X_{pre}(k)\|_{W_X}^2 \\ + \sum_{k=1}^{N_P} \|Y(k) - Y_{pre}(k) - d\|_{W_Y}^2 \\ + \|\mathbf{Y}_{N_p}(k) - \mathbf{Y}_{des}(k)\|_{\mathbf{Q}}^2 \\ + \|\Delta \mathbf{\bar{Z}}_{N_c}(k)\|_{\mathbf{R}}^2 + \|\varepsilon_k\|_{\mathbf{P}}^2 \end{aligned} \quad (31)$$

$$s.t. (k = 1, \dots, N_P)$$

$$\mathbf{\bar{X}}(k) = \mathbf{A} \mathbf{\bar{X}}(k-1) + \mathbf{B} \mathbf{\bar{Z}}_{N_c}(k-1) \quad (32)$$

$$\mathbf{\bar{Y}}(k) = \mathbf{C} \mathbf{\bar{X}}(k) + \mathbf{D} \mathbf{\bar{Z}}_{N_c}(k) \quad (33)$$

$$\mathbf{\bar{Y}}_s(k) = \mathbf{C}_s \mathbf{\bar{X}}(k) + \mathbf{D}_s \mathbf{\bar{Z}}_{N_c}(k) \quad (34)$$

$$\mathbf{\bar{Y}}_s(k) \leq \mathbf{\bar{Y}}_{s-\max} + \varepsilon_k \quad (35)$$

$$\varepsilon_k \geq 0 \quad (36)$$

$$\varepsilon_{k+1} = \varepsilon_k, k \neq c_1 N_{rs} + 1, c_1 = 1, \dots, N_P / N_{rs} \quad (37)$$

$$\mathbf{v}(k) \notin sVO(E_V^i, k) \quad (38)$$

$$\mathbf{v}(N_P) \notin GVO(E_V^i, N_P) \quad (39)$$

$$a \leq x(k) \leq b \quad (40)$$

$$v_{\min}(k) \leq v(k) \leq v_{\max}(k) \quad (41)$$

$$\theta_{\min}(k) \leq \theta(k) \leq \theta_{\max}(k) \quad (42)$$

$$RV = \left\{ \mathbf{v}(t) = (v(t), \theta(t)) \mid v(t) \in [v(t_0) + \dot{v}_{\min} \Delta t, v(t_0) + \dot{v}_{\max} \Delta t], \theta(t) \in [\theta(t_0) + \dot{\theta}_{\min} \Delta t, \theta(t_0) + \dot{\theta}_{\max} \Delta t] \right\} \quad (15)$$

$$FV = \left\{ \mathbf{v}(t) \mid \mathbf{v}(t) \in RV, \mathbf{v}(t) \notin GVO(E_V^i), \mathbf{v}(t) \notin ROV \right\} \quad (16)$$

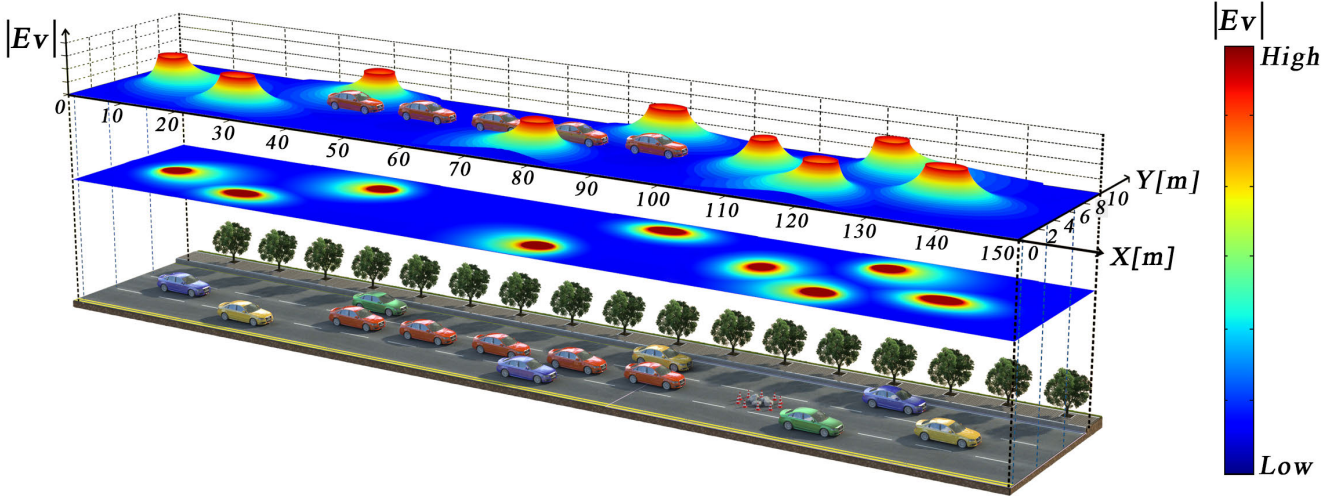


Fig. 6. Illustration of CAV platoon to avoid collision risks caused by multiple obstacles (set $G = 0.5$, $R = 1$, $K = 5$, $T = 1$, $\zeta = 1.2$).

$$\dot{v}_{\min}(k) \leq \Delta v(k) \leq \dot{v}_{\max}(k) \quad (43)$$

$$\dot{\theta}_{\min}(k) \leq \Delta \theta(k) \leq \dot{\theta}_{\max}(k) \quad (44)$$

$$\Delta \mathcal{Z}_{N_c}(k) = \Delta \mathcal{Z}_{N_c}(k-1), k \geq N_c, k \neq c_2 N_{rc} + N_c, \quad (45)$$

$$c_2 = 1, \dots, (N_p - N_c) / N_{rc} \quad (46)$$

$$\left(\frac{F_{xT}}{F_{xT_max}} \right)^2 + \left(\frac{F_{yf}}{F_{yf_0_max}} \cdot \frac{Wl_r}{WL_r - F_{xT}h} \right)^2 \leq \mu^2 \quad (47)$$

$$\left(\frac{F_{xT}}{F_{xT_max}} \right)^2 + \left(\frac{F_{yr}}{F_{yr_0_max}} \cdot \frac{Wl_f}{WL_f - F_{xT}h} \right)^2 \leq \mu^2 \quad (48)$$

$$F_{xT} \leq T_{max} / R_{eff} \quad (49)$$

where the multiobjective function consists of collision risk, control output, violation of the control input, slack variable, and the longitudinal and lateral errors of the predictive trajectory between the subject vehicle and its preceding vehicle.

Q , R , P , W_X , and W_Y are weighting factors of the above sub-objectives. X_{pre} and Y_{pre} are the lateral and longitudinal position of preceding vehicle. d denotes the space headway between two consecutive vehicles in a vehicle platoon.

Equation (32) and Equation (33) respectively predict the vehicle motion states and tracking outputs, where A , B , C , and D are the discrete state, input, output, and feedforward matrices. The constraint variables \mathcal{Y}_S are linearized as a function of states and inputs in Equation (34), where C_S and D_S are the output and feedforward matrices. Equation (35)-(37) presents the constraints on the vehicle actuators, motion speed, and corresponding linear constraints of the tire capacity constraints.

Equation (38) and (39) guide the subject vehicle to select the free-collision velocities. Equation (40) constrains the subject vehicle to drive within the driveable area. The reachable velocity and angle are constrained in Equation (41)-(44), where v_{\min} and v_{\max} and θ_{\min} and θ_{\max} are the lower and upper bounds of velocity and steering angle. Equation (45) constrains the number of the control inputs to save computation costs.

The lateral and longitudinal tire force constraints are presented in Equation (46)-(48), where F_{xT} is the tire longitudinal force, F_{xT_max} is the maximum tire longitudinal force, F_{yf} and F_{yr} is the front and rear lateral tire force, F_{yf0_max} and F_{yf0_max} is the nominal maximum lateral rear and front tire force, W is the vehicle weight, h is the height of the vehicle's center of gravity from the ground, T_{max} is the maximum propelling torque, R_{eff} is the radius of the wheels.

At each time step, the MPC-based controller continuously observes the real-time driving environment information of the subject vehicle (platoon vehicle or adaptive cruise vehicle), predicts the trajectory of the obstacle vehicle, and computes the collision risk magnitude and distribution around the subject vehicle within the predicted time horizon. Once the collision risk magnitude of the subject vehicle exceeds a specified threshold at any time step, the collision avoidance path planning algorithm is triggered. The generalized velocity obstacle algorithm is utilized to compute the collision velocity sets sVO and GVO . The dynamic window approach is employed to determine the feasible velocity set FV . Subsequently, the cost function is solved to generate the optimal collision-avoidance path and velocity. The resulting control scheme is then outputted for execution by the subject vehicle. In a dynamic environment, if the driving environment information surrounding the subject vehicle remains unchanged or the altered CRPF intensity does not exceed the threshold in future time steps, the subject vehicle will persist in executing the current control scheme. Otherwise, the MPC-based controller updates the CRPF, sVO and GVO , FV , and control scheme based on environmental changes and trends. The updated control scheme is then outputted to the subject vehicle for execution. The MPC-based controller is iteratively executed at each time step until the subject vehicle successfully avoids the collision risk. The MPC-based optimisation problem Equation (30) and (31) are solved by the MATLAB embedded function 'fmincon'. the Sequential Quadratic Programming (SQP) algorithm is utilized to optimize the cost function, while the interior-point algorithm handles the constraints.

Please note that the incorporation of the velocity obstacle theory significantly improves the solution efficiency of these MPC algorithms. The velocity obstacle theory identifies and predicts the potential collision space and the dynamics of the collision avoidance solution set in the long-term domain. This reduces the search space of alternative solutions and the computational time required for calculations. Moreover, the velocity obstacle theory employs collision space instead of collision points to estimate the collision velocity set, thereby addressing the issue of frequent long-term collision alarms caused by underestimating the collision velocity set. The MPC algorithm eliminates the need for the solution process and reduces the computational cost associated with underestimating the obtained collision solution.

V. HYBRID AUTOMATON MODELING FOR SYSTEM COLLABORATION

Multiple independent maneuvers need a synergistic mechanism to realize their flexible transition and operation. Existing algorithms fail to avoid instruction-retrieval exceptions and maneuver-transition interruptions due to non-uniform system settings [21], [40]. This section proposes a hybrid automaton architecture to achieve the collaboration and transition of platoon merging and splitting.

A. Hybrid Automaton Architecture

A hybrid automaton is introduced to model the hybrid system with continuous states and discrete events [55]. Each discrete event has its continuous states, and the state evolves by interleaving pieces of continuous execution with discrete transitions. The hybrid automaton architecture considered in this study is defined as a tuple Q , as shown in Equation (48).

$$Q = \langle Manv, VehSta, ConInt, ConOut, Event, TranProc, SubSyst, SubCons, SubInit \rangle \quad (50)$$

where,

$Manv = \{Cruising, Pllooning\}$ is a finite set of maneuvers that represent control modes of the hybrid system. Cruising and Pllooning represent single-vehicle cruising and multiple-vehicle platooning, respectively.

$VehSta = [Y \ v_y \ X \ v_x \ \theta \ r]$ is a state vector of the hybrid system related to the subject vehicle and its neighbouring vehicles.

$ConInt = [F_{yT} \ \delta]$ is a control input vector for the subject vehicle consisting of the total tire longitudinal force and the steering angle of its front wheels.

$ConOut = [X \ v_y \ \theta]$ is a control out vector for the subject vehicle consisting of lateral position, longitudinal velocity, and direction angle.

$Event = \{MERGE, SPLIT\}$ is an event set of system transitions, including platoon merging and splitting.

$SubSyst, SubCons, SubInit, TranProc$ represent discrete maneuver's continuous control subsystems, operation constraints, initial conditions, and transition process, respectively.

B. Motion States

To accurately track the operation and transmission of system states, the motion states of the subject vehicle and the obstacle vehicle are defined interactively.

1) *Subject Vehicle's Motion States*.: Subject vehicle's motion information is mainly related to its longitudinal and lateral locations, velocity vector, acceleration vector, and platoon states. A string of this information is defined as Equation (49).

2) *Obstacle Vehicle's Motion States*.: Obstacle vehicle's motion information is mainly related to vehicle type, longitudinal and lateral locations, velocity vector, acceleration vector, and relative information for a subject vehicle. A string of this information is defined with respect to a specific subject vehicle, as shown in Equation (50).

$$VehState = \left\{ \begin{array}{l} VehID, VehLoP, VehLaP, VehSpd, \\ VehAng, VehAcc, VehAngAcc, \\ PltnDumy, PltnID, PltnNum, \\ PltnHdwy, PltnSpd, PrecedID \end{array} \right\} \quad (51)$$

$$VehState = \left\{ \begin{array}{l} ObID, ObLoP, ObLaP, \\ ObSpd, ObAng, ObAcc, \\ ObAngAcc, ReltSpd, ReltAng, \\ ReltDis, ObCRPF, ObPrty \end{array} \right\} \quad (52)$$

where, $VehID$ is a subject vehicle's identifier, $VehLoP$, $VehLaP$, $VehSpd$, $VehAng$, $VehAcc$, $VehAngAcc$ represent subject vehicle's longitudinal and lateral locations, speed, speed angle (i.e., motion direction), acceleration, and acceleration angle, respectively. $PltnDumy$ is a platooning enable flag which is 1 when the subject vehicle is allowed to merge a platoon, and 0 when it only cruises alone. $PltnID$ is a platoon's identifier which is 0 when there is only one single-cruising vehicle, or is the composition of the platooning vehicles' ID tail numbers. $PltnNum$, $PltnHdwy$, $PltnSpd$, and $PrecedID$ represent the platoon's total number of vehicles, preset space headway and speed, and an identifier of subject vehicle's preceding vehicle, respectively.

C. Maneuver-Transition Rules

$ObID$ is an obstacle vehicle's identifier, $ObLoP$, $ObLaP$, $VehSpd$, $ObAng$, $ObAcc$, $ObAngAcc$ represent longitudinal and lateral locations, speed, speed angle, acceleration, and acceleration angle, respectively. $ReltSpd$, $ReltAng$, $ReltDis$, $ObCRPF$ represent the relative speed, azimuth angle, distance, and collision risk strength, respectively. $ObPrty$ represents the priority of the specific subject vehicle to handle the obstacle.

Fig. 7 depicts the maneuver transition process modeled by the hybrid automaton. Under the initial conditions, the subject vehicle operates in either the single-vehicle cruising or multiple-vehicle platooning subsystem. The operational objectives defined by Equations (30) and (31) guide the behaviors of the two subsystems. Upon the activation of a maneuver transition signal, the control constraints and goals for the subject vehicle are adjusted through platoon merging or splitting. The subject vehicle adjusts its maneuver mode

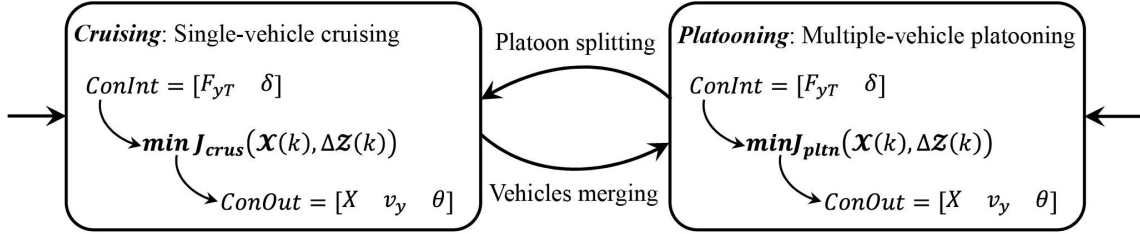


Fig. 7. Maneuver transition modelled by the hybrid automaton.

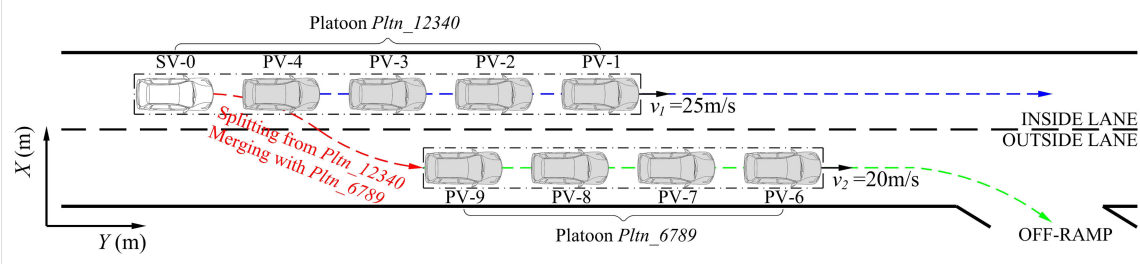


Fig. 8. Illustration for the event-trigger rule of platoon splitting and merging.

TABLE I
VARIATION OF VEHICLE MOTION STATES BEFORE AND AFTER THE SPLIT TRANSITION

VehID	Transition	PlatoonID	PltnDumy	PrecedID	PltnNum	PltnSpd	Manv	Function
PV-1	Before	Pltn_12340	1	0	5	25m/s	Platooning	J_{pltn}
	After	Pltn_1234	1	0	4	25m/s	Platooning	J_{pltn}
PV-2	Before	Pltn_12340	1	PV-1	5	25m/s	Platooning	J_{pltn}
	After	Pltn_1234	1	PV-1	4	25m/s	Platooning	J_{pltn}
PV-3	Before	Pltn_12340	1	PV-2	5	25m/s	Platooning	J_{pltn}
	After	Pltn_1234	1	PV-2	4	25m/s	Platooning	J_{pltn}
PV-4	Before	Pltn_12340	1	PV-3	5	25m/s	Platooning	J_{pltn}
	After	Pltn_1234	1/0	PV-3	4	25m/s	Platooning	J_{pltn}
SV-0	Before	Pltn_12340	1/0	PV-4	5	25m/s	Platooning	J_{pltn}
	After	0	1/0	0	1	20m/s	Cruising	J_{crus}

from the current subsystem to another based on the updated instructions.

D. Event-Trigger Rules

Platoon splitting and merging are crucial events in the cooperative platoon control system. This section provides detailed explanations of the modeling process for these two events in the hybrid automaton. Fig. 8 illustrates the modeling process for platoon splitting and merging.

1) *Platoon Splitting Event*: During the platoon splitting event, a subject vehicle in a multiple-vehicle platoon continuously monitors the motion state of its preceding vehicle and the surrounding driving environment for changes. If the driving conditions no longer meet the requirements for platoon-following driving, a split signal will be triggered for the subject vehicle to separate from the current platoon. The subject vehicle modifies its motion states to separate from the current platoon. TABLE I displays the changes in vehicle motion states before and after the split transition.

2) *Vehicle Merging Event*: A single-cruising vehicle or a platooning vehicle following behind a platoon can be considered as a candidate for forming a new platoon. The subject vehicle constantly monitors the motion state of the candidate vehicle. If the car-following speed and headway requirements are met, a merge signal will be activated to form a new platoon with the candidate vehicle. The subject vehicle

modifies its motion states to follow the candidate vehicle with the appropriate speed and headway. TABLE II shows the changes in vehicles' motion states before and after the merge transition.

VI. NUMERICAL ANALYSIS

A. Numerical Estimation of the Collision-Warning Thresholds

Vehicles often do not take immediate collision-avoidance measures upon detecting a collision risk. The vehicle will continue driving in its current motion state until the collision risk reaches a collision-warning threshold, such as a warning time or risk threshold. The collision-warning threshold serves as a trigger switch for activating the collision avoidance and motion planning algorithms in the subject vehicle. This threshold plays a pivotal role in enabling timely actions to ensure the safety of the subject vehicle [56], [57]. Smaller thresholds assist in maintaining the expected vehicle movement but elevate the risk of collision. Conversely, larger thresholds enhance collision avoidance, albeit at the cost of increased travel delays caused by deviations from the desired path. Thus, the setting of the collision-warning threshold must strike a balance between traffic safety and driving efficiency.

Fig. 9 illustrates the collision-warning time and the collision risk threshold. As shown in Fig. 9 (a), the velocities in $S1$ will lead to a higher collision risk before the collision-warning time t_{Thres} , the velocity in $S2$ will lead to a higher collision risk

TABLE II
VARIATION OF VEHICLE MOTION STATES BEFORE AND AFTER THE SPLIT TRANSITION

VehID	Transition	PlatoonID	PltnDumy	PrecedID	PltnNum	PltnSpd	Manv	Function
PV-6	Before	Pltn_6789	1	0	4	20m/s	Platooning	J_{pltn}
	After	Pltn_67890	1	0	5	20m/s	Platooning	J_{pltn}
PV-7	Before	Pltn_6789	1	PV-6	4	20m/s	Platooning	J_{pltn}
	After	Pltn_67890	1	PV-6	5	20m/s	Platooning	J_{pltn}
PV-8	Before	Pltn_6789	1	PV-7	4	20m/s	Platooning	J_{pltn}
	After	Pltn_67890	1	PV-7	5	20m/s	Platooning	J_{pltn}
PV-9	Before	Pltn_6789	1/0	PV-8	4	20m/s	Platooning	J_{pltn}
	After	Pltn_67890	1	PV-8	5	20m/s	Platooning	J_{pltn}
SV-0	Before	0	1/0	0	1	25m/s	Cruising	J_{crus}
	After	Pltn_67890	1/0	PV-9	5	20m/s	Platooning	J_{pltn}

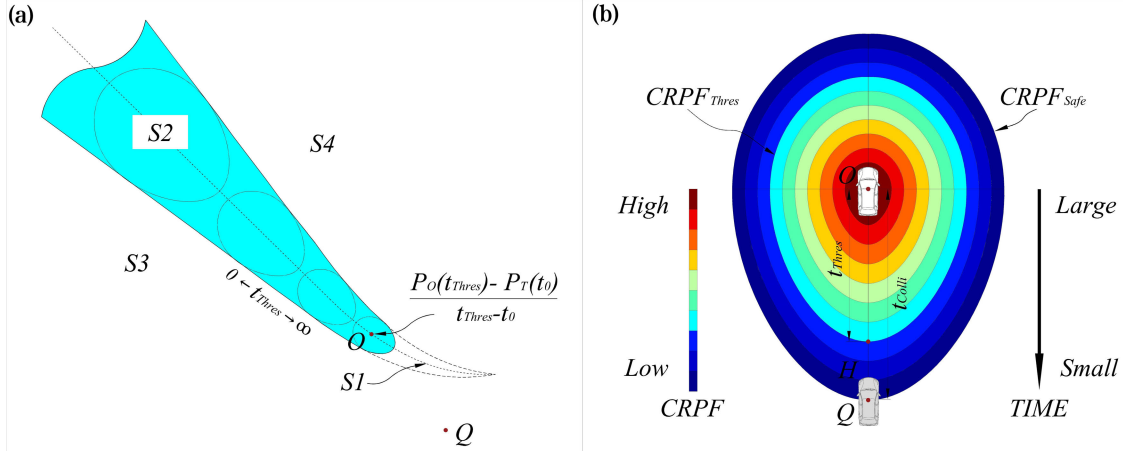


Fig. 9. Illustration of CRPF threshold based on a nonlinear GVO set. (a) Time threshold-based candidate velocity space, (b) Time threshold-based CRPF threshold.

after the time t_{Thres} the velocities in $S3$ will lead the subject vehicle to pass the collision area by the rear of the obstacle vehicle, and the velocities in $S4$ will lead the subject vehicle to pass the collision area by the front of the obstacle vehicle.

The collision-warning time can well describe the collision risk in the rear-end direction of two successive vehicles. The collision risk threshold can be designated as the collision risk at the location of the collision-warning time from obstacle vehicles. As shown in Fig. 9 (b), the subject vehicle will collide with the obstacle vehicle at point O in time of t_{Coll} . The subject vehicle reaches the collision-warning time t_{Thres} at point H . The collision risk threshold $CRPF_{Thres}$ is the collision risk at point H . The candidate velocity distribution in Fig. 9 (a) can be determined by the equipotential line with risk $CRPF_{Thres}$.

Fig. 10 illustrates a series of numerical experiments conducted to evaluate the performance of various collision-warning times. The safety and efficiency of obstacle vehicles are evaluated for different collision-warning times under various motion states, including constant speed (acceleration = 0), deceleration (acceleration = $-0.5m/s^2$), and acceleration (acceleration = $0.5m/s^2$). Safety performance is evaluated using two metrics: the minimum Time-to-Collision (TTC) [58], [59] and the Time Exposed Time-to-Collision (TET) [60]. Efficiency performance is assessed by measuring the deviations in location and velocity between the actual and desired paths. The numerical results are presented in Fig. 10 (b) and (c).

Increasing the collision-warning time results in larger values of minimum TTC and lower values of TET. During

the test with the obstacle vehicle driving at a constant speed, the minimum TTC exceeds the collision threshold of $TTC = 2.0s$ [56], [57], [58], and the TET remains at 0 when the collision-warning time is equal to or greater than 2.2s. The decreasing rate of velocity deviation becomes less pronounced starting from a collision-warning time of 2.2s, resulting in a relatively low location deviation of $12.84m/s$ at a collision-warning time of 2.2s (second only to $11.77m/s$ at 2.1s).

The test results indicate similar outcomes for obstacle vehicles with decelerating or accelerated motion. The collision risk may vary in different vector positions of the obstacle vehicle under the same threshold strength in different motion states, but the conflict strength for the subject vehicle remains constant. Consequently, the subject vehicle exhibits a consistent level of urgency and operability in taking measures to avoid the collision risk. Hence, the collision-warning time threshold is specified as 2.2s. Therefore, the collision risk threshold is set the collision risk with $TTC = 2.2s$.

B. Numerical Experiments of the Proposed Hybrid Automaton Architecture

1) *Experiment Design:* Two numerical experiments are designed to verify the performance of the proposed hybrid automaton architecture.

• *Experiment 1: nonlinear obstacle avoidance.* This experiment aims to test the feasibility of the hybrid automaton architecture to avoid nonlinear motion obstacles. As shown in Fig. 11(a), there were four lanes in the simulation road,

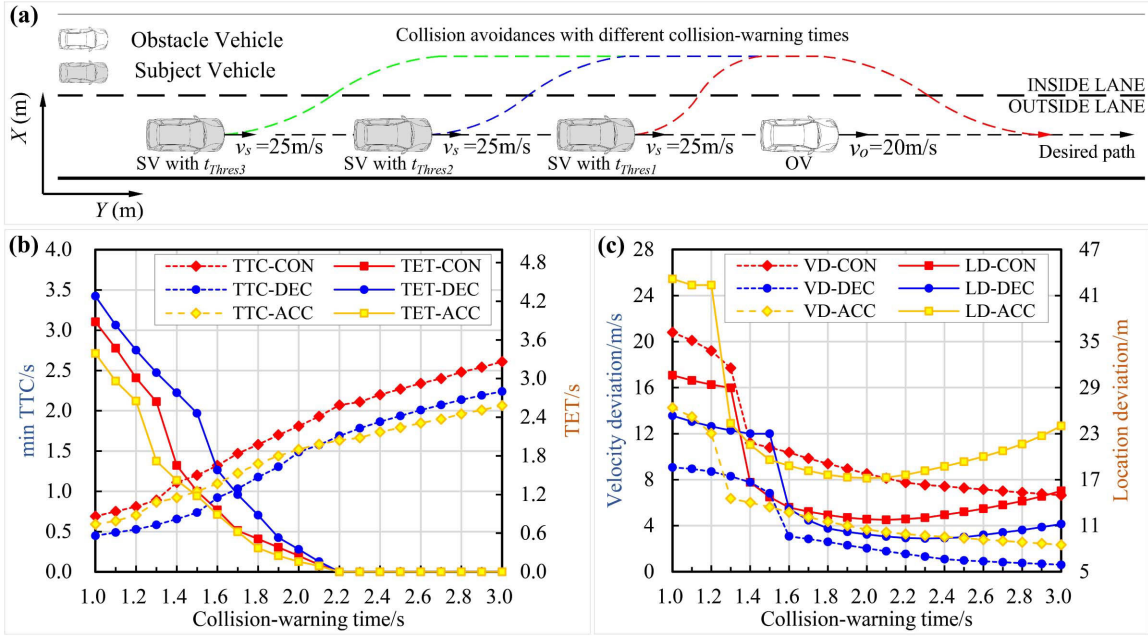


Fig. 10. Estimation of the safety and efficiency performances of different collision-warning times. (a) Illustration of the case study, (b) Safety performance, (c) Efficiency performance. Note: Location deviation $LD = \sum_{i=1}^{i=T} \Delta l_i = \sum_{i=1}^{i=T} \sqrt{(x_{iR} - x_{iD})^2 + (y_{iR} - y_{iD})^2}$, Velocity deviation $VD = \sum_{i=1}^{i=T} \Delta v_i = \sum_{i=1}^{i=T} |v_{iR} - v_{iD}|$. CON: constant speed; DEC: deceleration; ACC: acceleration.

including two mainline lanes, one off-ramp lane, and one auxiliary lane transitioning from the mainline to the off-ramp. The lane width was 4m. A five-vehicle platoon drives at 25m/s on lane-2. An obstacle vehicle changes lane from lane-1 toward the off-ramp with a longitudinal speed of 22m/s and a lateral acceleration of -0.5 m/s^2 . The subject platoon may need to split to avoid the obstacle vehicle and then remerge into the vehicle platoon.

To examine the impact of communication delay on the control performance of the proposed algorithm, several experiments were conducted with different communication delays, following the approach outlined in previous studies [61], [62]. Communication delays of 0s, 0.025s, 0.050s, 0.075s, and 0.100s were tested, representing different scenarios.

- *Experiment 2: multiple obstacles avoidance.* This experiment is designed to test the hybrid automaton architecture's performance to avoid multiple obstacles. As shown in Fig. 11(b), two lanes were set up, and the width of each lane was 4m. A five-CAV platoon drives at 25m/s on lane-2. An obstacle vehicle OV-1 drives with a lower speed of 23m/s on lane-2. Another obstacle vehicle OV-2 drives at 24m/s on lane-1 in front of OV-1. The subjective platoon may need to conduct a double lane-changing to overtake the two obstacle vehicles.

To test the control performance of the architecture in complex situations, two emergency cases two emergency scenarios involving obstacle vehicles operating in a stop-and-go manner are set up. In Case 1, OV-1 initially decelerated at -2.0 m/s^2 for 2s, followed by an acceleration of 1.0 m/s^2 for 4s, and eventually maintained a constant speed. In Case 2, OV-2 initially decelerated at -1.0 m/s^2 for 3s, followed by an acceleration of 1.5 m/s^2 for 2s, and eventually maintained a constant speed.

It should be noted that the subject vehicle has more than two actions when avoiding obstacles, including longitudinal deceleration/acceleration and lane change. In practical situations, vehicles are often reluctant to change lanes. When vehicles detect a collision risk, they initially avoid the obstacle vehicle by decelerating and making slight adjustments to the lateral position. Only when the slight adjustment is insufficient to achieve collision avoidance, the vehicle will gradually increase the range of lateral position adjustment until a lane change is necessary. This approach has been widely adopted and applied in numerous studies [19], [21], [30], [41]. Consequently, the proposed algorithm enables vehicles to avoid collision risks by making slight adjustments to the lateral position.

The intelligent driving model (IDM) and the trinomial trajectory model (TTM) are employed to model vehicles' car-following and lane-changing behaviors. IDM and TTM have been widely used in the simulation of CAV behaviors [58], [63]. TABLE III summarizes the vehicle maneuver parameters and the control architecture settings [41], [42]. The resulting average calculation time of the optimization problem per time step using a personal computer with an Intel Core i7-8650U CPU @ 1.90 GHz, 16 GB RAM, and 512 GB SSD is 0.0134s. It is notable that since the step time is 0.05m/s, the optimization problem can be solved in real time.

2) Experiment Results of Nonlinear Obstacle Avoidance:

Fig. 12 shows the control responses of platoon vehicles to avoid the nonlinear obstacle vehicle. The perceived collision risk of the leading vehicle (SV-1) reached the collision risk threshold at 4.0s (see Fig. 12 (a)). SV-1 fell into the velocity obstacle from the obstacle vehicle (see Fig. 12 (h)). Since the obstacle vehicle was not significantly moving to the right, SV-1 adopted successive accelerations to drive away from the velocity obstacle space (see Fig. 12 (e)). As the obstacle vehicle intensified its rightward movement, SV-1 is unable to fully

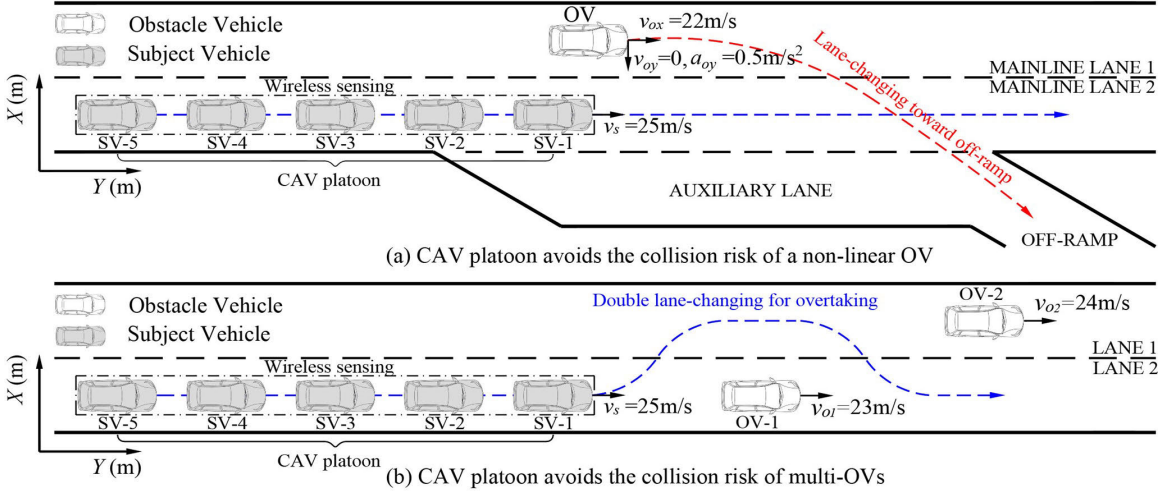


Fig. 11. Illustration of the numerical experiment scenarios for the proposed hybrid automaton architecture.

TABLE III
SYSTEM PARAMETERS IN THE SIMULATION SCENARIOS

Parameter	Value	Parameter	Value	Parameter	Value	Parameter	Value
G	0.5	R	1	ζ	1.2	T_{max}	3000Nm
I_Z	4600Kgm ²	μ	0.9	l_r	1.434m	h	0.647m
l_f	1.421m	C_f	127000N	K	5	T	1
$v_{a,max}$	4.0m/s ²	$v_{d,max}$	4.8m/s ²	$\dot{v}_{a,com}$	1.4m/s ²	F_{xT_max}	20000N
F_{yf0_max}	10400N	F_{yr0_max}	10600N	N_P	20	N_C	5
$\dot{\theta}_a$	1.0deg	$\dot{\theta}_d$	-1.0deg	W	2270kg	t_{Thres}	2.2s

TABLE IV

EFFECT OF COMMUNICATION DELAY ON SAFETY PERFORMANCE OF THE AUTOMATON ARCHITECTURE

Communication delay	min TTC (s)	TET(s)
$C_D=0s$	2.18	0
$C_D=0.025s$	2.15	0
$C_D=0.050s$	2.10	0
$C_D=0.075s$	1.94	1.08
$C_D=0.100s$	1.66	2.12

avoid the obstacle vehicle through longitudinal adjustment. Collision risk and desired path drove SV-1 turned right slightly to reduce the collision risk caused by its following vehicle and the obstacle vehicle (see Fig. 12 (b)). SV-1 gradually moved away from the obstacle vehicle collision risk area. And the desired path drove SV-1 back to the desired path and gradually decelerates to the desired speed. As shown in Fig. 12 (h2), SV-1 drove out of the velocity obstacle from the obstacle vehicle at 4.5s. SV-2 performed a similar response to SV-1 to avoid the obstacle vehicle.

As shown in Fig. 12 (b), there was not enough space for SV-3 to avoid the collision risk by following its preceding vehicle SV-2. SV-3 had to split from the platoon by decreasing its longitudinal speed and slightly adjusting its lateral position to the left (see Fig. 12 (f) and Fig. 12 (g)). This is related to the simultaneous adjustment of the horizontal and vertical motion states to enable SV-3 to drive away from obstacles more effectively in the long-term domain. And it may be related to SV-3 avoiding the increased risk of collision with its following vehicle SV-4. As the obstacle vehicle significantly moved to the right, the collision risk between SV-3 and the obstacle vehicle gradually decreased (see Fig. 12 (a)). SV-3 gradually reduced the adjustment amplitude of the lateral

position (see Fig. 12 (f)). After the collision risk were further reduced, the desired path drove SV-3 rightward to the desired lateral position (see Fig. 12 (b)). Then, a series of acceleration actions were taken to reduce the space from SV-2 after driving out of the velocity obstacle at 6.5s (see Fig. 12 (h4)). Finally, SV-3 recovered the desired speed of 25m/s and remerged with SV-2 at 17s (see Fig. 12 (e)). SV-4 and SV-5 did not fall into the obstacle velocity space of the obstacle vehicle. They shifted motion states and trajectories to follow their preceding vehicles. Finally, the five subject vehicles remerged into the vehicle platoon and drove away from the simulation area.

As depicted in Fig. 13, the collision avoidance performance of the proposed algorithm gradually decreases as the communication delay increases. Specifically, when the communication delay $C_D \leq 0.050s$, the proposed algorithm can effectively guide the subject vehicle to exit the conflict velocity space with the obstacle vehicle (see Fig. 13 (a1)-(a4) and (b1)-(b4)) and the high-risk area (see Fig. 13 (a) and (b)). However, for communication delays $C_D \geq 0.075s$, certain subject vehicles occasionally fail to timely exit the high-risk collision space with obstacle vehicles (see Fig. 13 (c) and (d)). The number of vehicles and the duration of their delay in exiting the conflict space also increase with the rise in communication delay (see Fig. 13 (c1) and (d1)-(d3)).

TABLE IV presents the impact of communication delay on the safety performance of the hybrid automaton architecture. With an increase in communication delay, the minimum TTC during vehicle collision avoidance gradually rises. Importantly, when the communication delay is 0.05s, the minimum TTC exceeds 2.0s and the TET remains at 0s throughout the entire collision avoidance process. These findings demonstrate that

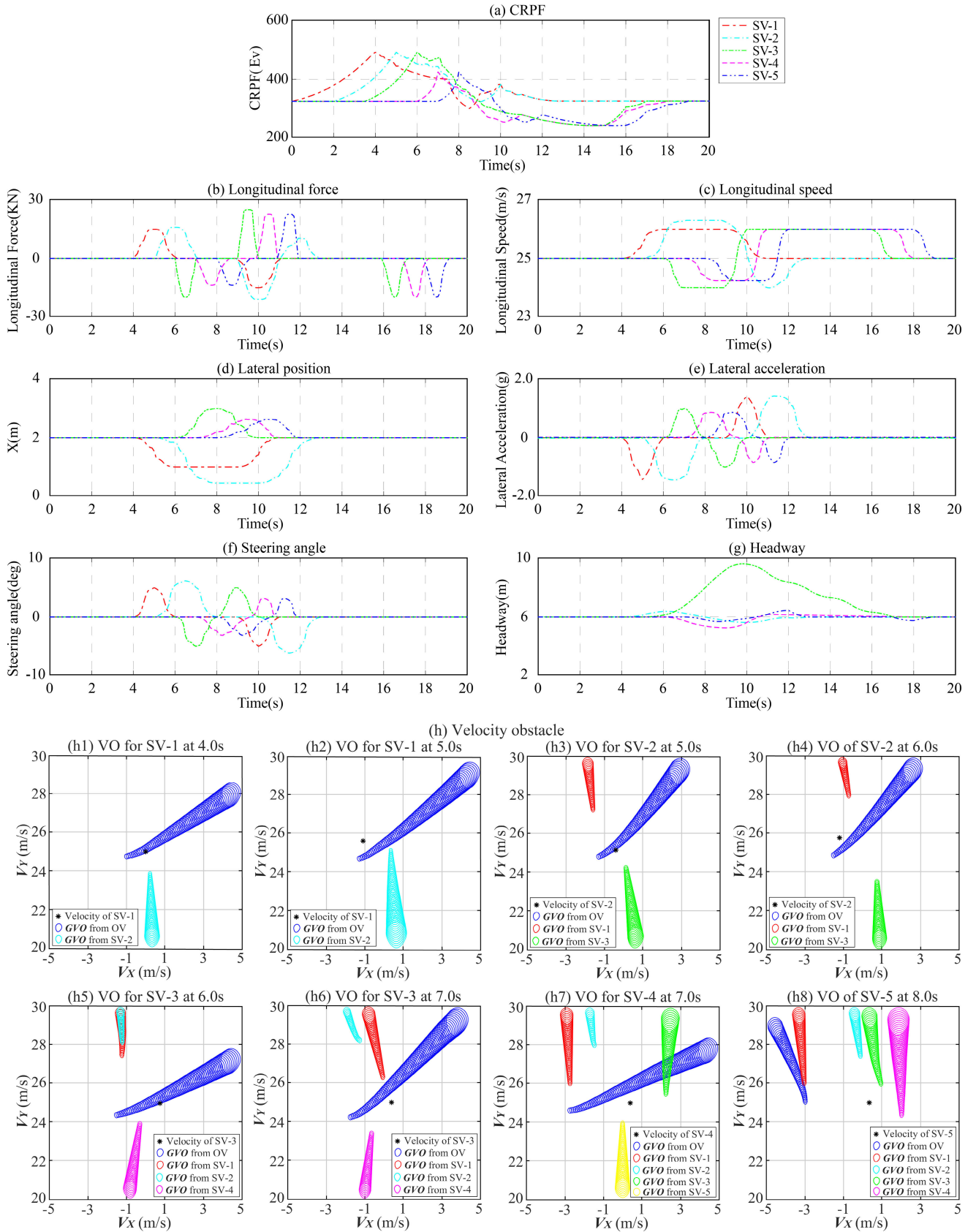


Fig. 12. Control response of the hybrid automaton architecture in response to the nonlinear obstacle. (a) Perceived CRPF strength, (b) Motion trajectory, (c) Space headway, (d) Longitudinal force, (e) Longitudinal speed, (f) Lateral acceleration, (g) Steering angle, (h) Encountered velocity obstacle.

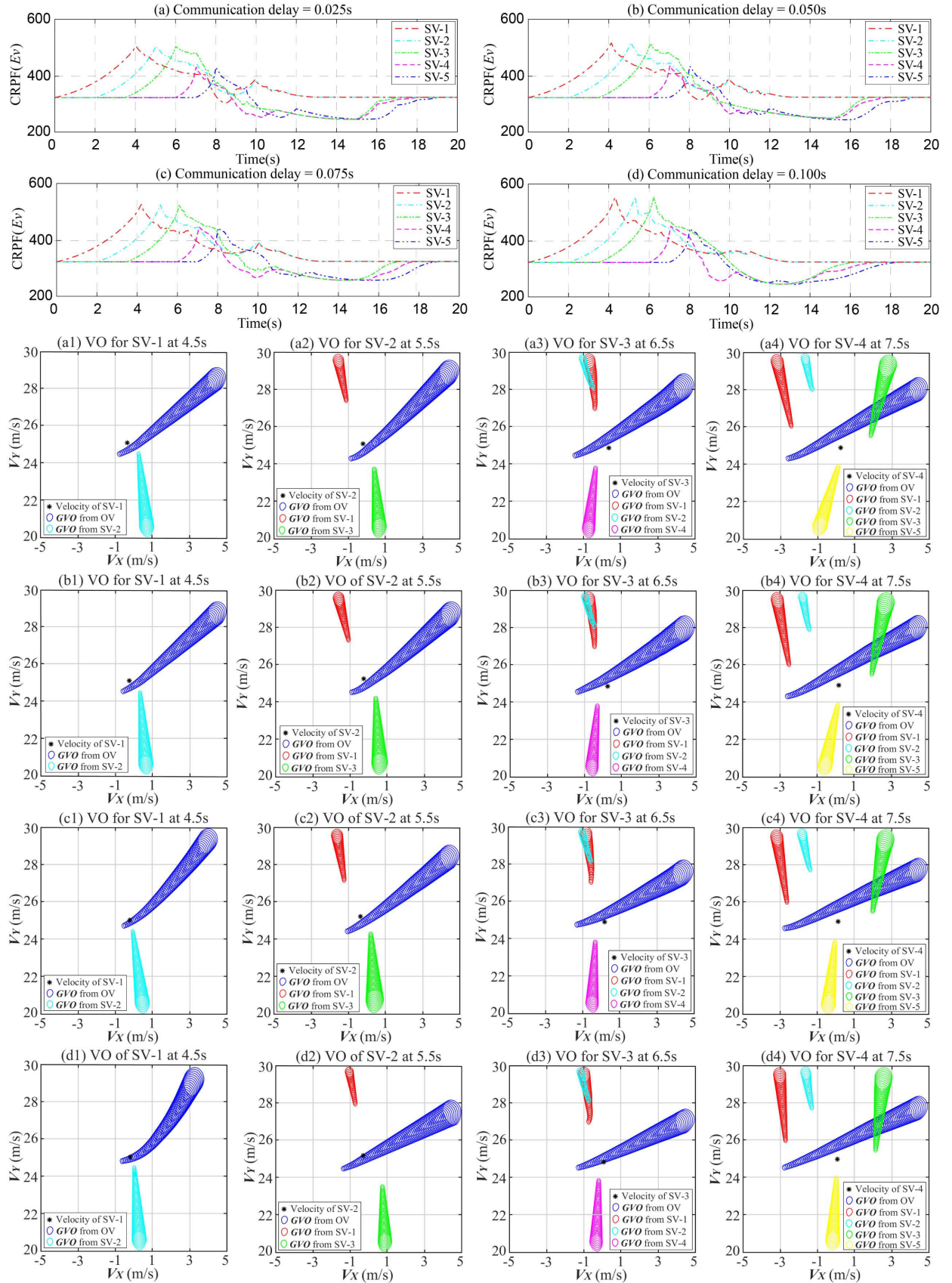


Fig. 13. Control performance of the hybrid automaton architecture with different communication delay.

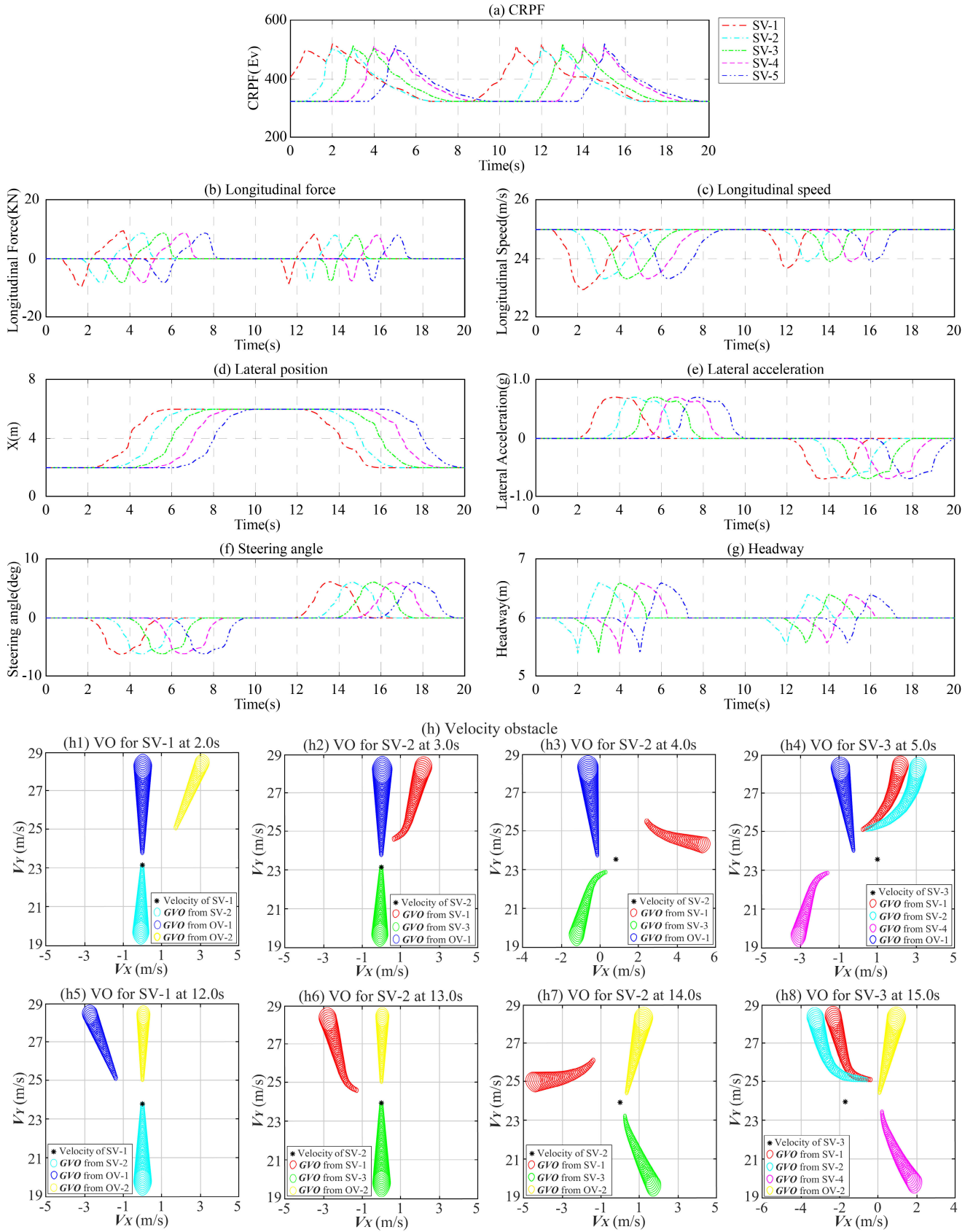


Fig. 14. Control response of the hybrid automaton architecture in response to multiple obstacles. (a) Perceived CRPF strength, (b) Motion trajectory, (c) Space headway, (d) Longitudinal force, (e) Longitudinal speed, (f) Lateral acceleration, (g) Steering angle, (h) Encountered velocity obstacle.

the control performance of the proposed collision avoidance algorithm can be ensured in a connected environment with a

communication delay $C_D \leq 0.05s$. The above results highlight the robustness of the proposed algorithm in mitigating

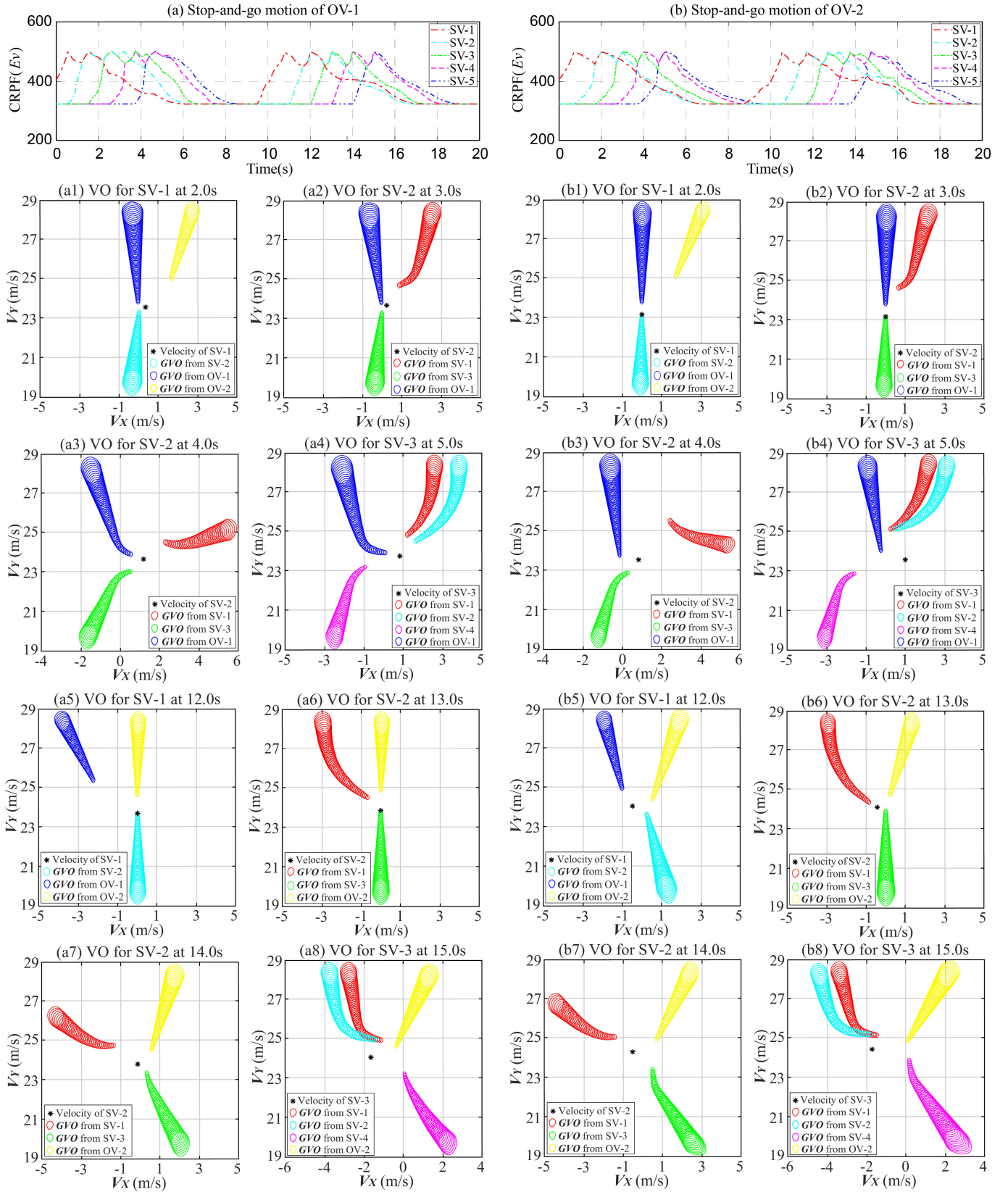


Fig. 15. Control performance of the hybrid automaton architecture in response to stop-and-go obstacles in emergency situations.

collision risks in a communication delay environment [61], [62].

The control responses demonstrate that the proposed collision detection algorithm accurately identifies evolving

collision risks and provides appropriate velocity solutions. The proposed motion planning algorithm effectively guides vehicle platoons to navigate around nonlinear obstacles. The hybrid automaton architecture successfully facilitates the maneuver

TABLE V

SAFETY MEASUREMENT OF THE HYBRID AUTOMATON
ARCHITECTURE IN MULTI-OBSTACLE SITUATIONS

Communication delay	min TTC (s)	TET(s)
Constant motion of obstacles	2.19	0
Stop-and-go motion of OV-1	2.12	0
Stop-and-go motion of OV-2	1.65	0

transition of platoon splitting and merging in the collision avoidance process.

(3) Experiment results of multiple obstacles avoidance

Fig. 14 illustrates the control responses of the vehicle platoon in avoiding multiple obstacle vehicles. The perceived collision risk of the leading vehicle (SV-1) reached the collision risk threshold at 0.8s (see Fig. 14 (a)). SV-1 continuously reduced its speed to mitigate the collision risk posed by the first obstacle vehicle (OV-1) (see Fig. 14 (d) and Fig. 14 (e)). The distance between SV-1 and its following vehicle (SV-2) decreased, and SV-1 became trapped in the velocity obstacle from SV-2 at 2.0s (see Fig. 14 (h1)). Sequential lateral maneuvers were executed to navigate away from the velocity obstacle and decrease the collision risks associated with OV-1 and SV-2 (see Fig. 14 (b) and Fig. 14 (g)).

The collision risk caused by the second obstacle vehicle (OV-2) exceeded the threshold again at 10.9s, and SV-1 became trapped in the velocity obstacle from SV-2 at 12.0 seconds. SV-1 modified its lateral trajectory by increasing acceleration to avoid collisions with OV-1, OV-2, and SV-2. The desired path directed SV-1 towards the centerline of lane-1 with a reduced steering angle. The other vehicles in the platoon followed their respective leading vehicles to adjust their motion trajectories. They navigated out of the velocity obstacles and high-risk areas consecutively. Eventually, all vehicles in the platoon regained their desired motion states and exited the simulation area as a platoon.

Fig. 15 shows the control performance of the hybrid automaton architecture in response to emergency obstacles. The collision detection algorithm accurately identifies the collision risk posed by the two stop-and-go obstacles. The collision velocity distribution for each subject vehicle is identified in the long-term horizon. The proposed motion planning algorithm guides subject vehicles to effectively and timely escape from high-risk conflict spaces. For example, SV-1 is trapped in the high-risk collision space of OV-1 at 0.5s (see Fig. 15 (a)), and SV-2 falls into the velocity obstacle of SV-3 at 3.0s in case 2 (see Fig. 15 (b2)). The proposed motion planning algorithm successfully enables SV-1 and SV-2 to escape their collision velocity set at 2.0s and 4.0s, respectively (see Fig. 15 (a1) and Fig. 15 (b3)).

TABLE V shows safety measurement of the hybrid automaton architecture in response to these emergency situations. Throughout the entire collision avoidance process, the minimum TTC exceeds 2.0s and the TET remains at 0s. This finding suggests that the proposed hybrid automaton architecture effectively guides all subject vehicles to safely avoid emergency obstacles. The hybrid automaton architecture demonstrates robustness in handling emergency obstacle avoidance.

The experimental results validate the effectiveness of the proposed collision detection algorithm in accurately detecting collision risks from multiple obstacles and generating collision-free velocity solutions. The motion planning algorithm demonstrates accurate tracking of vehicle motion states and trajectories during the collision avoidance process. Moreover, the hybrid automaton architecture exhibits excellent performance in adjusting the formation of the vehicle platoon to accommodate changing driving environments.

VII. CONCLUSION

This study proposed a three-layer hybrid automation architecture for CAV platoons to effectively avoid collision risks. The architecture comprised an upper layer for module unification and coordination, a middle layer for collision detection and avoidance, and a lower layer for motion planning and tracking. To validate the effectiveness of the proposed hybrid automaton architecture, two numerical experiments were conducted in a connected vehicle environment, considering nonlinear and multiple obstacles. The experimental results validate the performance of the control architecture and demonstrate its capability to address collision risks in CAV platoons.

Results demonstrate the effectiveness of the proposed collision detection algorithm in accurately identifying collision risks and providing velocity solutions. The motion planning algorithm exhibits strong performance in optimizing trajectories for both single-cruising vehicles and multiple-vehicle platoons. Moreover, the developed hybrid automaton architecture showcases its flexibility in successfully executing maneuver transitions between single-vehicle cruising and multiple-vehicle platooning during the collision avoidance process. The designed hybrid automaton also excels in adjusting the formation of the vehicle platoon to accommodate collision avoidance and motion planning requirements. The architecture shows outstanding performance in addressing collision risks, motion planning, and platoon formation adjustment.

This study can be enhanced by addressing the following research tasks. Firstly, the consideration of vehicle platoon stability is crucial for ensuring internal safety within vehicle platoons. Integrating platoon stability considerations into motion planning algorithms is expected to enhance the operational safety of vehicle platoons. Secondly, as the application of CAV technology progresses, there will be a transition period with a mixed traffic flow consisting of both CAVs and manually driven vehicles. Further development of the hybrid automaton architecture should consider the unique characteristics of mixed traffic flows. Also, incorporating field vehicle trajectory data to refine the collision risk threshold can improve the practicality and applicability of the proposed control architecture for collision avoidance in real-world vehicle scenarios. Moreover, the computational efficiency demanded by the control algorithm is crucial in influencing its performance, and future research can thoroughly investigate and assess its impact with a large amount of field data. Last but not least, it is important to consider the potential challenges posed by communication failures, such as random link outages, communication latency, and packet loss, in the design and

implementation of collision avoidance algorithms. Addressing these factors can significantly enhance the control robustness of these algorithms in connected environments.

REFERENCES

- [1] G. Ma, B. Wang, and S. S. Ge, "Robust optimal control of connected and automated vehicle platoons through improved particle swarm optimization," *Transp. Res. C, Emerg. Technol.*, vol. 135, Feb. 2022, Art. no. 103488.
- [2] Y. Wu, S. E. Li, J. Cortés, and K. Poolla, "Distributed sliding mode control for nonlinear heterogeneous platoon systems with positive definite topologies," *IEEE Trans. Control Syst. Technol.*, vol. 28, no. 4, pp. 1272–1283, Jul. 2020.
- [3] Y. Guo, T. Sayed, and L. Zheng, "A hierarchical Bayesian peak over threshold approach for conflict-based before-after safety evaluation of leading pedestrian intervals," *Accident Anal. Prevention*, vol. 147, Nov. 2020, Art. no. 105772.
- [4] B. Zhang, E. S. Wilschut, D. M. C. Willemse, and M. H. Martens, "Transitions to manual control from highly automated driving in non-critical truck platooning scenarios," *Transp. Res. F, Traffic Psychol. Behav.*, vol. 64, pp. 84–97, Jul. 2019.
- [5] S. Woo and A. Skabardonis, "Flow-aware platoon formation of connected automated vehicles in a mixed traffic with human-driven vehicles," *Transp. Res. C, Emerg. Technol.*, vol. 133, Dec. 2021, Art. no. 103442.
- [6] A. Duret, M. Wang, and A. Ladino, "A hierarchical approach for splitting truck platoons near network discontinuities," *Transp. Res. Proc.*, vol. 38, pp. 627–646, Jan. 2019.
- [7] R. Liu, Y. Ren, H. Yu, Z. Li, and H. Jiang, "Connected and automated vehicle platoon maintenance under communication failures," *Veh. Commun.*, vol. 35, Jun. 2022, Art. no. 100467.
- [8] H. Xing, J. Ploeg, and H. Nijmeijer, "Smith predictor compensating for vehicle actuator delays in cooperative ACC systems," *IEEE Trans. Veh. Technol.*, vol. 68, no. 2, pp. 1106–1115, Feb. 2019.
- [9] Y. Wang, R. Su, and B. Wang, "Optimal control of interconnected systems with time-correlated noises: Application to vehicle platoon," *Automatica*, vol. 137, Mar. 2022, Art. no. 110018.
- [10] Y. Liu et al., "Joint communication and computation resource scheduling of a UAV-assisted mobile edge computing system for platooning vehicles," *IEEE Trans. Intell. Transp. Syst.*, vol. 23, no. 7, pp. 8435–8450, Jul. 2022.
- [11] J. Wang, S. Gong, S. Peeta, and L. Lu, "A real-time deployable model predictive control-based cooperative platooning approach for connected and autonomous vehicles," *Transp. Res. B, Methodol.*, vol. 128, pp. 271–301, Oct. 2019.
- [12] H. Guo, J. Liu, Q. Dai, H. Chen, Y. Wang, and W. Zhao, "A distributed adaptive triple-step nonlinear control for a connected automated vehicle platoon with dynamic uncertainty," *IEEE Internet Things J.*, vol. 7, no. 5, pp. 3861–3871, May 2020.
- [13] A. Ibrahim, D. Goswami, H. Li, I. M. Soroa, and T. Basten, "Multi-layer multi-rate model predictive control for vehicle platooning under IEEE 802.11p," *Transp. Res. C, Emerg. Technol.*, vol. 124, Mar. 2021, Art. no. 102905.
- [14] M. Li, Z. Li, S. Wang, and B. Wang, "Anti-disturbance self-supervised reinforcement learning for perturbed car-following system," *IEEE Trans. Veh. Technol.*, vol. 72, no. 9, pp. 11318–11331, Sep. 2023.
- [15] H. Zhang, L. Du, and J. Shen, "Hybrid MPC system for platoon based cooperative lane change control using machine learning aided distributed optimization," *Transp. Res. B, Methodol.*, vol. 159, pp. 104–142, May 2022.
- [16] T. Zeng, O. Semiahi, W. Saad, and M. Bennis, "Joint communication and control for wireless autonomous vehicular platoon systems," *IEEE Trans. Commun.*, vol. 67, no. 11, pp. 7907–7922, Nov. 2019.
- [17] C. Chen, J. Wang, Q. Xu, J. Wang, and K. Li, "Mixed platoon control of automated and human-driven vehicles at a signalized intersection: Dynamical analysis and optimal control," *Transp. Res. C, Emerg. Technol.*, vol. 127, Jun. 2021, Art. no. 103138.
- [18] J. Wu, S. Ahn, Y. Zhou, P. Liu, and X. Qu, "The cooperative sorting strategy for connected and automated vehicle platoons," *Transp. Res. C, Emerg. Technol.*, vol. 123, Feb. 2021, Art. no. 102986.
- [19] C. Somarakis, Y. Ghaedsharaf, and N. Motiee, "Risk of collision and detachment in vehicle platooning: Time-delay-induced limitations and tradeoffs," *IEEE Trans. Autom. Control*, vol. 65, no. 8, pp. 3544–3559, Aug. 2020.
- [20] W. J. Scholte, P. W. A. Zegelaar, and H. Nijmeijer, "A control strategy for merging a single vehicle into a platoon at highway on-ramps," *Transp. Res. C, Emerg. Technol.*, vol. 136, Mar. 2022, Art. no. 103511.
- [21] G. C. Calafiore, C. Possieri, and A. V. Proskurnikov, "Collision-avoiding decentralized control for vehicle platoons: A mechanical perspective," *IFAC-PapersOnLine*, vol. 53, no. 2, pp. 15235–15240, 2020.
- [22] J. Lygeros, D. N. Godbole, and S. Sastry, "Verified hybrid controllers for automated vehicles," *IEEE Trans. Autom. Control*, vol. 43, no. 4, pp. 522–539, Apr. 1998.
- [23] C. J. Tomlin, J. Lygeros, and S. Shankar Sastry, "A game theoretic approach to controller design for hybrid systems," *Proc. IEEE*, vol. 88, no. 7, pp. 949–970, Jul. 2000.
- [24] P. Nilsson et al., "Correct-by-construction adaptive cruise control: Two approaches," *IEEE Trans. Control Syst. Technol.*, vol. 24, no. 4, pp. 1294–1307, Jul. 2016.
- [25] Y. Zhu and F. Zhu, "Barrier-function-based distributed adaptive control of nonlinear CAVs with parametric uncertainty and full-state constraint," *Transp. Res. C, Emerg. Technol.*, vol. 104, pp. 249–264, Jul. 2019.
- [26] W. J. Scholte, P. W. A. Zegelaar, and H. Nijmeijer, "Gap opening controller design to accommodate merges in cooperative autonomous platoons," *IFAC-PapersOnLine*, vol. 53, no. 2, pp. 15294–15299, 2020.
- [27] R. Kianfar, P. Falcone, and J. Fredriksson, "A control matching model predictive control approach to string stable vehicle platooning," *Control Eng. Pract.*, vol. 45, pp. 163–173, Dec. 2015.
- [28] J. Ligthart, E. Semsar-Kazerooni, J. Ploeg, M. Alirezaei, and H. Nijmeijer, "Controller design for cooperative driving with guaranteed safe behavior," in *Proc. IEEE Conf. Control Technol. Appl. (CCTA)*, Aug. 2018, pp. 1460–1465.
- [29] A. Alam, A. Gattami, K. H. Johansson, and C. J. Tomlin, "Guaranteeing safety for heavy duty vehicle platooning: Safe set computations and experimental evaluations," *Control Eng. Pract.*, vol. 24, pp. 33–41, Mar. 2014.
- [30] C. Zhai, Y. Liu, and F. Luo, "A switched control strategy of heterogeneous vehicle platoon for multiple objectives with state constraints," *IEEE Trans. Intell. Transp. Syst.*, vol. 20, no. 5, pp. 1883–1896, May 2019.
- [31] X. Ge, Q.-L. Han, J. Wang, and X.-M. Zhang, "Scalable and resilient platooning control of cooperative automated vehicles," *IEEE Trans. Veh. Technol.*, vol. 71, no. 4, pp. 3595–3608, Apr. 2022.
- [32] D. Lee, S. Lee, Z. Chen, B. B. Park, and D. H. Shim, "Design and field evaluation of cooperative adaptive cruise control with unconnected vehicle in the loop," *Transp. Res. C, Emerg. Technol.*, vol. 132, Nov. 2021, Art. no. 103364.
- [33] J. Chen, H. Liang, J. Li, and Z. Xu, "A novel distributed cooperative approach for mixed platoon consisting of connected and automated vehicles and human-driven vehicles," *Phys. A, Stat. Mech. Appl.*, vol. 573, Jul. 2021, Art. no. 125939.
- [34] H. G. Tanner, A. Jadbabaie, and G. J. Pappas, "Flocking in fixed and switching networks," *IEEE Trans. Autom. Control*, vol. 52, no. 5, pp. 863–868, May 2007.
- [35] A. D. Ames, X. Xu, J. W. Grizzle, and P. Tabuada, "Control barrier function based quadratic programs for safety critical systems," *IEEE Trans. Autom. Control*, vol. 62, no. 8, pp. 3861–3876, Aug. 2017.
- [36] Y. Chen, H. Peng, and J. Grizzle, "Obstacle avoidance for low-speed autonomous vehicles with barrier function," *IEEE Trans. Control Syst. Technol.*, vol. 26, no. 1, pp. 194–206, Jan. 2018.
- [37] J. Wang, J. Wu, and Y. Li, "The driving safety field based on driver-vehicle-road interactions," *IEEE Trans. Intell. Transp. Syst.*, vol. 16, no. 4, pp. 2203–2214, Aug. 2015.
- [38] R. Raja, A. Dutta, and K. S. Venkatesh, "New potential field method for rough terrain path planning using genetic algorithm for a 6-wheel rover," *Robot. Auto. Syst.*, vol. 72, pp. 295–306, Oct. 2015.
- [39] L. Li, J. Gan, X. Ji, X. Qu, and B. Ran, "Dynamic driving risk potential field model under the connected and automated vehicles environment and its application in car-following modeling," *IEEE Trans. Intell. Transp. Syst.*, vol. 23, no. 1, pp. 122–141, Jan. 2022.
- [40] Z. Huang, D. Chu, C. Wu, and Y. He, "Path planning and cooperative control for automated vehicle platoon using hybrid automata," *IEEE Trans. Intell. Transp. Syst.*, vol. 20, no. 3, pp. 959–974, Mar. 2019.
- [41] Y. Rasekhipour, A. Khajepour, S.-K. Chen, and B. Litkouhi, "A potential field-based model predictive path-planning controller for autonomous road vehicles," *IEEE Trans. Intell. Transp. Syst.*, vol. 18, no. 5, pp. 1255–1267, May 2017.

- [42] S. Wang, Z. Li, B. Wang, J. Ma, and J. Yu, "Velocity obstacle-based collision avoidance and motion planning framework for connected and automated vehicles," *Transp. Res. Rec., J. Transp. Res. Board*, vol. 2676, no. 5, pp. 748–766, May 2022.
- [43] X. Xiong, J. Sha, and L. Jin, "Optimizing coordinated vehicle platooning: An analytical approach based on stochastic dynamic programming," *Transp. Res. B, Methodol.*, vol. 150, pp. 482–502, Aug. 2021.
- [44] P. Fiorini and Z. Shiller, "Motion planning in dynamic environments using velocity obstacles," *Int. J. Robot. Res.*, vol. 17, no. 7, pp. 760–772, Jul. 1998.
- [45] P. Chen, Y. Huang, E. Papadimitriou, J. Mou, and P. H. A. J. M. van Gelder, "An improved time discretized non-linear velocity obstacle method for multi-ship encounter detection," *Ocean Eng.*, vol. 196, Jan. 2020, Art. no. 106718.
- [46] G. A. Mercado Velasco, C. Borst, J. Ellerbroek, M. M. van Paassen, and M. Mulder, "The use of intent information in conflict detection and resolution models based on dynamic velocity obstacles," *IEEE Trans. Intell. Transp. Syst.*, vol. 16, no. 4, pp. 2297–2302, Aug. 2015.
- [47] Y. Huang, P. H. A. J. M. van Gelder, and Y. Wen, "Velocity obstacle algorithms for collision prevention at sea," *Ocean Eng.*, vol. 151, pp. 308–321, Mar. 2018.
- [48] J. Wang, J. Wu, X. Zheng, D. Ni, and K. Li, "Driving safety field theory modeling and its application in pre-collision warning system," *Transp. Res. C, Emerg. Technol.*, vol. 72, pp. 306–324, Nov. 2016.
- [49] H. Yukawa, "On the interaction of elementary particles. I," *Proc. Physico-Math. Soc. Jpn. 3rd Ser.*, vol. 17, pp. 48–57, Jan. 1935.
- [50] D. Fox, W. Burgard, and S. Thrun, "The dynamic window approach to collision avoidance," *IEEE Robot. Autom. Mag.*, vol. 4, no. 1, pp. 23–33, Mar. 1997.
- [51] E. J. Molinos, Á. Llamazares, and M. Ocaña, "Dynamic window based approaches for avoiding obstacles in moving," *Robot. Auto. Syst.*, vol. 118, pp. 112–130, Aug. 2019.
- [52] V. Havu and J. Malinen, "The Cayley transform as a time discretization scheme," *Numer. Funct. Anal. Optim.*, vol. 28, nos. 7–8, pp. 825–851, Aug. 2007.
- [53] S. J. Qin and T. A. Badgwell, "A survey of industrial model predictive control technology," *Control Eng. Pract.*, vol. 11, no. 7, pp. 733–764, Jul. 2003.
- [54] Y. Huang, H. Wang, A. Khajepour, H. He, and J. Ji, "Model predictive control power management strategies for HEVs: A review," *J. Power Sources*, vol. 341, pp. 91–106, Feb. 2017.
- [55] R. Alur et al., "The algorithmic analysis of hybrid systems," *Theor. Comput. Sci.*, vol. 138, no. 1, pp. 3–34, 1995.
- [56] Y. Guo, M. Essa, T. Sayed, M. M. Haque, and S. Washington, "A comparison between simulated and field-measured conflicts for safety assessment of signalized intersections in Australia," *Transp. Res. C, Emerg. Technol.*, vol. 101, pp. 96–110, Apr. 2019.
- [57] T. Liu, Z. Li, P. Liu, C. Xu, and D. A. Noyce, "Using empirical traffic trajectory data for crash risk evaluation under three-phase traffic theory framework," *Accident Anal. Prevention*, vol. 157, Jul. 2021, Art. no. 106191.
- [58] S. Wang, Z. Li, Z. Cao, A. Jolfaei, and Q. Cao, "Jam-absorption driving strategy for improving safety near oscillations in a connected vehicle environment considering consequential jams," *IEEE Intell. Transp. Syst. Mag.*, vol. 14, no. 2, pp. 41–52, Mar. 2022.
- [59] M. Li, Z. Cao, and Z. Li, "A reinforcement learning-based vehicle platoon control strategy for reducing energy consumption in traffic oscillations," *IEEE Trans. Neural Netw. Learn. Syst.*, vol. 32, no. 12, pp. 5309–5322, Dec. 2021.
- [60] W. Shun-chao, L. Zhi-bin, W. Yao, W. Bing-tong, and L. Meng, "An intelligent jam-absorbing driving strategy for eliminating multiple traffic oscillations at bottlenecks," *China J. Highway Transp.*, vol. 35, no. 1, p. 137, 2022.
- [61] Z. Yang, J. Huang, D. Yang, and Z. Zhong, "Collision-free ecological cooperative robust control for uncertain vehicular platoons with communication delay," *IEEE Trans. Veh. Technol.*, vol. 70, no. 3, pp. 2153–2166, Mar. 2021.
- [62] L. Xu, W. Zhuang, G. Yin, and C. Bian, "Energy-oriented cruising strategy design of vehicle platoon considering communication delay and disturbance," *Transp. Res. C, Emerg. Technol.*, vol. 107, pp. 34–53, Oct. 2019.
- [63] Q. Guo, X. Ban, and H. M. A. Aziz, "Mixed traffic flow of human driven vehicles and automated vehicles on dynamic transportation networks," *Transp. Res. C, Emerg. Technol.*, vol. 128, Jul. 2021, Art. no. 103159.



Shunchao Wang received the B.Eng. degree from Shandong Jiaotong University in 2016, the M.Eng. degree from the Beijing University of Technology in 2019, and the Ph.D. degree from the School of Transportation, Southeast University, China, in 2023. He is currently a Post-Doctoral Researcher with Southeast University. His research interests include traffic flow modeling, cooperative control of connected and automated vehicles, collision avoidance motion planning, traffic safety modeling, and travel behavior modeling.



Zhibin Li received the Ph.D. degree from the School of Transportation, Southeast University, China, in 2014. From 2010 to 2012, he was a Visiting Student with the University of California at Berkeley, Berkeley, CA, USA. From 2015 to 2017, he was a Post-Doctoral Researcher with the University of Washington and The Hong Kong Polytechnic University. He is currently a Professor with Southeast University. His research interests include intelligent transportation and traffic control. He received the Best Doctoral Dissertation Award from the China Intelligent Transportation Systems Association in 2015. He was selected as the World's Top 2% Scientists and Highly Cited Chinese Researchers by Elsevier in 2021 and 2022.



Bingtong Wang received the M.Eng. degree in transportation engineering from Lanzhou Jiaotong University, China, in 2019. He is currently pursuing the Ph.D. degree with the School of Transportation, Southeast University. He has authored many articles published in top-tier journals, such as *Transportation Research Part B: Methodological*. His research interests include traffic flow modeling, traffic control, intelligent traffic systems, connected and automated vehicle control, and traffic safety modeling.



Meng Li received the B.Eng. degree from the School of Transportation, Southeast University, China, in 2018, where he is currently pursuing the Ph.D. degree. He received the support of the Excellent Ph.D. Funding of Southeast University in 2021. He has authored many articles published in top-tier journals, such as *IEEE TRANSACTIONS ON NEURAL NETWORKS AND LEARNING SYSTEMS*, *IEEE TRANSACTIONS ON INTELLIGENT TRANSPORTATION SYSTEMS*, and *IEEE TRANSACTIONS ON VEHICULAR TECHNOLOGY*. His research interests include reinforcement learning and microscopic traffic flow modeling within the connected vehicle environment.